

MATHEMATICAL MODELING AND ANALYSIS OF WITHIN-HOST INFLUENZA INFECTION DYNAMICS

CASSANDRA WILLIAMS AND KRISTA WURSCHER

MAIN ADVISOR: BLESSING O. EMERENINI

SECONDARY ADVISOR: RICARDO N. G. REYES GRIMALDO

OREGON STATE UNIVERSITY

ABSTRACT. Influenza is a viral infectious disease of high importance and widely studied around the world. In this study we model the within-host transmission of influenza in a continuous deterministic setting (system of ordinary differential equations) and a discrete stochastic framework (discrete-time Markov chain model). Previous models omit cellular restoration through cellular death, which is a key component for the possibility of chronic infections. We thus investigate the effect of cellular restoration on the spread of influenza within the host. The conditions or existence of a disease-free equilibrium and biologically relevant endemic equilibrium are stated in terms of the basic reproductive number, \mathcal{R}_0 . When \mathcal{R}_0 is less than or equal to one the disease-free equilibrium was found to be locally asymptotically stable and the endemic equilibrium was unstable. For $\mathcal{R}_0 > 1$ the equilibrium behaviors were reversed, which is consistent with models that do not include cellular restoration. Finally, while Discrete-Time Markov Chains are rarely used in endemic models with more than two variables, we develop a method designing the necessary transition matrix to utilize DTMC instead of CTMC in endemic modeling.

1. INTRODUCTION

Influenza is a viral infectious respiratory disease that can be seasonal and mild, severe, or chronic. In 2018 there were 3-5 million cases of severe influenza around the world, resulting in approximately 500,000 deaths [1]. Part of what makes Influenza dangerous is that the virus mutates very quickly; in one day it can mutate more than humans have in the past several thousand years [20]. Influenza virus may

Date: August 16, 2019.

This work was done during the Summer of 2019 REU program in Mathematics and Theoretical Computer Science at Oregon State University supported by NSF grant DMS-1757995.

be contracted via an air-borne path by inhaling the cough droplets of an infected individual (in the case of human influenza), or a vector-borne virus that is contracted via infected birds (in the case of avian influenza). Human influenza attacks the upper respiratory tract; however, it is capable of spreading to cells in the lower respiratory tract, cardiovascular system, and nervous system. It is in these secondary locations that it is most dangerous [11]. Humans are primarily infected by either influenza A or influenza B. These two types of influenza are distinguishable by the rate the virus mutates. Individuals can sometimes develop immunity to influenza B for years, but due to the rate of mutation in influenza A, people are not able to develop immunity [11, 20].

Once an influenza viron makes it past the mucous membrane that covers organ tissue, it is trapped within the pericilliary fluid which makes direct contact with epithelial cells in the respiratory tract. The epithelium consists of four different types of cells: ciliated cells, non-ciliated cells, clara cells, and basal cells. Influenza usually targets ciliated cells and non-ciliated cells and binds to their cell surface receptors [35, 34, 39, 48, 53]. Viruses cannot replicate on their own, so they must hijack cells and utilize their genetic replication process [20]. Approximately 20 minutes after an influenza viron binds to the surface receptors of a cell, it is brought into the cell through endocytosis, allowing for viral genetic material to be sent to the nucleus where it is replicated and used to produce viral proteins [42, 271-297]. Once the viral proteins and genetic material are put together, new virions are sent out of the cell to infect other cells [5]. Thousands of new virions may be produced within 6 hours of the initial infection of a single cell [5, 20]. The presence of foreign bodies prompts the activation of interferons, which down-regulate viral production, and activate natural killer cells as part of the innate immune response [5, 43]. About 5 day post infection, the adaptive immune response kicks in and antigen-specific antibodies are detectable [8, 27, 36].

Most of the time, the infected cell will produce virions until its cell membrane is either consumed or the cell is destroyed by the immune system [5, 8]. Death is the most likely outcome for infected cells, however, a minority of infected cells are able to recover; these cells are called ‘survivor’ cells [16, 22]. Cells that have the ability to recover from influenza B infection are predominantly ciliated epithelial cells. After the infection has run its course, approximately 3% of the epithelial cells

can be labeled as survivor cells, 74% of which were ciliated, and are located primarily in the trachea [16]. The presence of these survivor cells has been shown to improve epithelial barrier function, have antiviral effects, increase lung compliance, and speed host recovery [16].

At peak infection, 30-50% of epithelial cells are killed [8]. The body recognizes areas of dead cells due to infection as an injury and responds using a process called cell restoration. Within the trachea, nearby epithelial cells move to the wound within 12-24 hours. 15-24 hours after the injury, these cells begin to de-differentiate, then proliferate to cover the surface where the dead cells were, which results in new healthy cells [12, 13, 14, 23, 49, 51]. This process produces new cells that may be susceptible to infection, and the susceptibility of these new cells can result in chronic influenza infections. Thus, it is important to incorporate cellular restoration into any mathematical model that should be able to produce mild, severe, or chronic infections.

Mathematical modelling has been used to study the spread of diseases throughout populations dating back to the work of Daniel Bernoulli (1700-1782) regarding the effectiveness of inoculation against smallpox [9]. Since then, similar but expanded upon techniques have been used to analyze diseases such as Tuberculosis, HIV, Influenza, West Nile Virus, and Zika. Disease transmission models are so important because they allow us to acquire useful public health information, such as epidemic severity, epidemic length, vaccine and quarantine effectiveness, and the necessary anti-viral drug quantity. We use mathematical models because this information is less accessible through typical experimental and statistical approaches due to the scale of epidemics and the lack of pertinent data available [31]. Deterministic and stochastic models are commonly used and we will discuss both types throughout this paper.

The use of mathematical models for the study of within-host viral kinetics is a newer but similar practice to population studies. Instead of human populations, we have populations of cells. The importance of modeling revolves on their capability to facilitate our understanding of the mechanisms of viral kinetics, advise treatment methods and provide insight towards immune response dynamics and drug effectiveness [7]. This practice can be seen in HIV models, as well as similar Hepatitis C virus (HCV) and Human papillomavirus (HPV) models, where viral load decline

in patients with antiviral drug therapy [5]. It is also present in deterministic HIV models that explore topical microbicide product properties and how they work to prevent the sexual transmission of infections [29].

The within-host kinetics of influenza have been studied through many variations of mathematical models. These models examine viral loads kinetics from infection data, analyze symptoms, help us understand immune response dynamics, explore the impact from different host and viral factors, and review the efficacy of different treatments [46]. Influenza models come in ranging complexity, considering few to substantial numbers of parameters and variables. Common parameters that are considered include the viral clearance rate, the lifespan of infected cells, the lifespan of a viron, the length of the latent/eclipse phase, the rate of epithelial cell regeneration, and the lifespan of the interferon [7]. There is always a give and take between the simplicity and complexity of a model. Simplicity allows for better analysis but may sacrifice specific biological factors while complexity includes more biological factors at the cost of more unknown values that need to be estimated. In our model we consider a cellular restoration rate (r_D), the rate at which target cells come into contact with virions (β), the length of the latent phase ($\frac{1}{\tau_E}$), the lifespan of an infected cell ($\frac{1}{\tau_I}$), and the production and clearance rates of virions (p and c).

Deterministic models are useful for larger populations, through differential or difference equations, they allow us to make informed predictions. They assume that the susceptible and infectious populations are functions of time [31]. Many within-host influenza kinetics models already exist. They consider different degrees of complexity.

On the simpler end, such are the models developed by Baccam et. al, the variables in their first model include are target/susceptible epithelial cells, infected cells, and level of viral titer; their second model expanded upon the first to include two classes of infected cells: latent cells, which are infected cells that do not actively produce virions; and actively producing cells. This divide was instituted to account for the time delay of viron production after a cell is initially infected. Their second model produced more accurate cell lifespan parameters [5]. These and similar models assume that the limited availability of target epithelial cells is what eventually eradicates the virus, but does not directly include the impact from any immune responses. Advantages of these include that much of the available viral titer data fits them. However, they do

not specify what biological factors are responsible for the limitation of target cells, which leads to different parameter values [46].

As influenza models begin increasing in complexity, they start introducing more immune response factors. The model developed by Miao et. al builds upon the variables of Baccam et al.'s first model, by now introducing cells immune to infection and cells that regenerate. This is through antibodies IgG and IgM, as well as effector CD8 T cells. These come into play through the rates in which target cells, infected cells, and viral titer values interact with each other. Beyond this, Miao et. al split the models into two phases: the first taking into account innate immune responses and the second considering adaptive immune responses. The advantage of this model is that it more accurately fits the common pattern of viral titer data containing two peaks [36]. Our model will consider cellular restoration but will not take immune response factors directly into account.

Stochastic models differ from deterministic models in that they do not produce a single outcome, but instead generate a probability distribution of outcomes. This inherent randomness is useful in circumstances in which there are complex factors that we will not be able to perfectly model, which is ideal for biological systems such as the within-host spread of influenza. We use stochastic models to predict likely paths the influenza infection may take within the human body.

Researchers have used a number of different stochastic techniques in the modeling of infectious diseases, including Continuous-Time Markov Chains [6, 52], Discrete-time Markov Chains [40], Wright-Fisher Model [55], stochastic differential equations [10], and stochastic simulations on adaptive random networks [41]. They have also been used in prediction simulations of flu outbreaks [37, 40]. It is possible for deterministic models to predict an epidemic, while simulations of a stochastic model of the same disease result in disease extinction. These differences in model output indicates that the stochasticity of the infection process can drastically change the outcome [10]. Using stochastic modeling will allow us to use parameter estimation to complement our deterministic model.

A number of biological processes for within-host spread of infections can be appropriately modeled using stochastic processes. In 2019, Zhao et al. found that the mutation of RNA viruses, such as influenza, and the onset of antiviral drug resistance arise through a stochastic evolutionary process [55]. Additionally, utilizing

Continuous-Time Markov Chains has revealed that a stochastic event at the start of an influenza infection may result in virus extinction before symptoms are even noticed [52].

Time-delays exist in between transitions of cells between exposed to infectious classes, and infectious to dead/recovered classes. Understanding these time-delays is important because the amount of time a cell spends in each phase affects the number of virions produced by that cell. Stochastic models have been used to model these time delays because the amount of time it takes to transition between these states depends on the virus strain, and the cell. Comparing various distributions for the time-delays have revealed that Normal and lognormal delays provide better fits to biological data [24].

2. DETERMINISTIC MODEL

2.1. Governing Equations: In this project we propose to study the disease interaction with cells. The cells are grouped into four classes: Target cells, T , Exposed cell, E , Infectious cells, I , and Dead cells D (see Figure 2.1). T , represent the cell population susceptible to infection. These cells transition to the exposed class at the rate β . Cells enter the target class at a rate r_D due to cellular restoration which is triggered by dead cells, D . Exposed cells, E represent the cells that have been infected but are not yet producing new virions. This class can also be referred to as the latent or eclipse class. This class gains cells from the target population and loses cells to the infectious class at a rate of $\frac{1}{\tau_E}$. Infectious cells, I , represent the class that actively produces new virions. It gains cells from the exposed class and loses cells to infection related death at a rate of $\frac{1}{\tau_I}$. Finally, Virus, V represents the virus. Infectious cells produce new virions at rate p and cells clear the virus at a rate c .

$$\begin{aligned}
 (1) \quad & \frac{dT}{dt} = -\beta TV + r_D D \\
 (2) \quad & \frac{dE}{dt} = \beta TV - \frac{E}{\tau_E} \\
 (3) \quad & \frac{dI}{dt} = \frac{E}{\tau_E} - \frac{I}{\tau_I} \\
 (4) \quad & \frac{dV}{dt} = pI - cV
 \end{aligned}$$

where

$$N = D + T + E + I \implies D = N - T - E - I$$

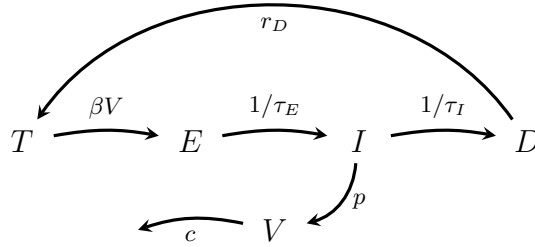


FIGURE 1. Compartmental diagram for model (1)-(4)

We conduct both a stability analysis and a sensitivity analysis on this model.

2.2. Steady states. We first find constant solutions (steady states) for system (1)-(4), by setting it equal to zero. This makes each derivative equal to zero, thus its integral produces a constant. We set all four of our rates simultaneously to zero and solve for the constant values of T , E , I , and V . The first thing we need to do is substitute $N - T - E - I$ in for D equation (1). N is a constant so this substitution lets us work with only our four variables.

Starting with (4), we algebraically manipulate it to isolate I and obtain an equation in terms of V with parameters c and p :

$$(5) \quad I = \frac{cV}{p}$$

Then, setting (3) equal to zero, algebraically isolating E , and substituting what we found in equation (2) in for I , we obtain an equation for E in terms of V with parameters c, p, τ_E and τ_I :

$$(6) \quad E = I \frac{\tau_E}{\tau_I} = \left(\frac{cV}{p} \right) \frac{\tau_E}{\tau_I}$$

Next we follow the same approach for (2) where we will isolate T . Set $\frac{dE}{dt}$ equal to zero, substitute what we found in equation (6) for E , cancel, and we obtain an equation for T . Due to the cancellation of V (thus $V \neq 0$), it is only in terms of the variables c, β, τ_I and p :

$$(7) \quad T = E \frac{1}{\beta V \tau_E} = \frac{cV \tau_E}{p \tau_I} \frac{1}{\beta V \tau_E} = \frac{c}{p \beta \tau_I}$$

Now we move on to the most involved equation, (1), which becomes the following when we substitute in for D :

$$\frac{dT}{dt} = -\beta TV + r_D(N - T - E - I)$$

First we substitute the values found in equations (7), (6), and (5) for T, E and I . Then we bring all the terms containing V to one side of the equation and all that do not contain V to the other. We factor out V and divide the remaining term to the other side. Finally, we simplify to obtain an equation for V based on all the parameters:

$$(8) \quad V = \frac{r_D(N\beta\tau_I p - c)}{c\beta(1 + r_D\tau_E + r_D\tau_I)}$$

Finally, we plug what we found for V back into equations (5) and (6) and we obtain the following **steady state equations**:

$$(9) \quad \begin{aligned} T &= \frac{c}{p\beta\tau_I} \\ E &= \frac{\tau_E r_D (N\beta\tau_I p - c)}{\tau_I p \beta (1 + r_D \tau_E + r_D \tau_I)} \\ I &= \frac{r_D (N\beta\tau_I p - c)}{p\beta (1 + r_D \tau_E + r_D \tau_I)} \\ V &= \frac{r_D (N\beta\tau_I p - c)}{c\beta (1 + r_D \tau_E + r_D \tau_I)} \end{aligned}$$

Notice that if $V = 0$, this implies (from equation (4)) that $I = 0$, thus $E = 0$ by equation (3) and finally $T = N$ by equation (1). We call this a Disease-Free Equilibrium (DFE).

2.3. Basic reproductive number, \mathcal{R}_0 . The basic reproductive number, \mathcal{R}_0 , tells us how many cells will be infected as a result of one infected cell (secondary cases per infected cell). If $\mathcal{R}_0 > 1$ the virus will grow, if $\mathcal{R}_0 < 1$ the virus will diminish, and if $\mathcal{R}_0 = 1$ then further analysis is required.

There are several different techniques to compute \mathcal{R}_0 but our approach will use the next generation matrix (NGM). First we take the Jacobian matrix of our system of equations:

$$(10) \quad J(\mathbf{X}) = \begin{pmatrix} -(\beta V + r_D) & -r_D & -r_D & -\beta T \\ \beta V & -\frac{1}{\tau_E} & 0 & \beta T \\ 0 & \frac{1}{\tau_E} & -\frac{1}{\tau_I} & 0 \\ 0 & 0 & p & -c \end{pmatrix}$$

Next, we plug in the conditions of our disease free equilibrium where the number of target cells is the total number of cells and everything else is zero, $T = N, E = I = V = 0$ and we now have:

$$(11) \quad J(N, 0, 0, 0) = J_{DFE} = \begin{pmatrix} -r_D & -r_D & -r_D & -\beta N \\ 0 & -\frac{1}{\tau_E} & 0 & \beta N \\ 0 & \frac{1}{\tau_E} & -\frac{1}{\tau_I} & 0 \\ 0 & 0 & p & -c \end{pmatrix}$$

This matrix can be expressed as the difference of a non-negative matrix \mathcal{F} and a non-singular Metzler matrix \mathcal{V} . By the work of Van den Driessche and Watmough [47] we can define the basic reproductive number R_0 as the spectral radius ρ of the matrix $\mathcal{F}\mathcal{V}^{-1}$ where:

$$(12) \quad \mathcal{F} = \begin{pmatrix} 0 & 0 & 0 & 0 \\ 0 & 0 & 0 & \beta N \\ 0 & \frac{1}{\tau_E} & 0 & 0 \\ 0 & 0 & p & 0 \end{pmatrix}$$

$$(13) \quad \mathcal{V} = \begin{pmatrix} r_D & r_D & r_D & \beta N \\ 0 & \frac{1}{\tau_E} & 0 & 0 \\ 0 & 0 & \frac{1}{\tau_I} & 0 \\ 0 & 0 & 0 & c \end{pmatrix}$$

$$(14) \quad \mathcal{V}^{-1} = \begin{pmatrix} \frac{1}{r_D} & -\tau_E & -\tau_I & -\frac{\beta N}{r_D c} \\ 0 & \tau_E & 0 & 0 \\ 0 & 0 & \tau_I & 0 \\ 0 & 0 & 0 & \frac{1}{c} \end{pmatrix}$$

Multiplying the matrices \mathcal{F} and \mathcal{V}^{-1} , we obtain:

$$(15) \quad \mathcal{F}\mathcal{V}^{-1} = \begin{pmatrix} 0 & 0 & 0 & 0 \\ 0 & 0 & 0 & \frac{\beta N}{c} \\ 0 & 1 & 0 & 0 \\ 0 & 0 & p\tau_I & 0 \end{pmatrix}$$

Setting $\det(\lambda I - \mathcal{F}\mathcal{V}^{-1})$ equal to zero, solving for λ , and taking the largest value, we obtain:

$$(16) \quad \rho(\mathcal{F}\mathcal{V}^{-1}) = \widetilde{\mathcal{R}}_0 = \left(\frac{\beta p N \tau_I}{c} \right)^{\frac{1}{3}}$$

2.4. Analysis of \mathcal{R}_0 . We can utilize equation (16) in a simplified form because all of our parameters are positive and we are comparing against 1. Thus our basic reproductive number is defined by:

$$(17) \quad \mathcal{R}_0 = \left(\frac{\beta p N \tau_I}{c} \right)$$

Next we express our steady state equations in terms of \mathcal{R}_0 so that we can explore what will happen when \mathcal{R}_0 is less than, equal to, or greater than one.

$$(18) \quad T = \frac{c}{p\beta\tau_I} \cdot \frac{\mathcal{R}_0}{\mathcal{R}_0} = \frac{\beta p N \tau_I}{p\beta\tau_I \mathcal{R}_0} = \frac{N}{\mathcal{R}_0} \quad \text{or} \quad \mathcal{R}_0 = \frac{N}{T}$$

Since the remaining equations contain the same term, $(N\beta\tau_I p - c)$, and since $c\mathcal{R}_0 = N\beta\tau_I p$, the term $(N\beta\tau_I p - c)$ can also be written as $c\mathcal{R}_0 - c$ or $c(\mathcal{R}_0 - 1)$. Substituting this in to our equilibrium equations for E, I and V , we have the following:

$$(19) \quad \begin{aligned} E &= (\mathcal{R}_0 - 1) \cdot \frac{\tau_E r_D}{\tau_I p \beta (1 + r_D \tau_E + r_D \tau_I)} \\ I &= (\mathcal{R}_0 - 1) \cdot \frac{r_D}{p \beta (1 + r_D \tau_E + r_D \tau_I)} \\ V &= (\mathcal{R}_0 - 1) \cdot \frac{r_D}{\beta (1 + r_D \tau_E + r_D \tau_I)} \end{aligned}$$

We have two cases to consider \mathcal{R}_0 .

Case 1: $\mathcal{R}_0 \leq 1$

The equation for T in terms of \mathcal{R}_0 , (18), tells us that $N < T$ and the similar equations for E, I and V , (19), tell us that E, I and V will all be negative. Both of these aspects are biologically irrelevant because T cannot exceed N and we cannot have negative cell populations. This tells us that the endemic equilibrium is unstable in this case.

However, our disease free equilibrium is relevant so we look at the biological implications of $\mathcal{R}_0 \leq 1$. Substituting in for the parameters that make up \mathcal{R}_0 , we obtain the inequality $\beta p N \leq c \frac{1}{\tau_I}$. This tells us that the maximum product of the rate target cells become exposed and viral production is less than or equal to the product of viral clearance and the lifespan of infected cells. In other words, the birth rate of the infection is less than or equal to the death rate of the infection. It makes sense that these conditions will lead to the disease free equilibrium.

Case 2: $\mathcal{R}_0 > 1$

Equation (18) tells us that $N > T$ and (19) tells us that E, I and V are all greater than zero. Both of these conditions are biologically relevant so we can consider this case further. Substituting in for the parameters that define \mathcal{R}_0 , we obtain the inequality $\beta p N \leq c \frac{1}{\tau_I}$. This tells us that the maximum product of the rate target cells become exposed and viral production is greater than the product of viral clearance and the lifespan of infected cells. Opposite from the case above, we have that the birth rate of infection is greater than the death rate of the infection, logically leading towards the endemic equilibrium.

The stability of the two equilibrium and its relationship with \mathcal{R}_0 will be addressed.

2.5. Boundary behavior. Our biological constraints dictate that only non-negative cell populations are relevant. We analyze the behavior of the system of differential equations on the T, E, I and V axes, all the combinations of planes, and all the combinations of hyper-planes, in order to confirm that solutions always point from the boundaries inward towards the set of positive real numbers of the state space, $\Omega = \{(T, E, I, V) \in \mathbb{R}^4 \mid 0 \leq T, E, I, V, \quad N \geq T + E + I\} \subset \mathbb{R}_+^4$.

Axis	T	$(T, 0, 0, 0) \rightarrow (r_D(N - T), 0, 0, 0)$
	E	$(0, E, 0, 0) \rightarrow (r_D(N - E), -\frac{E}{\tau_E}, \frac{E}{\tau_E}, 0)$
	I	$(0, 0, I, 0) \rightarrow (r_D(N - I), 0, -\frac{I}{\tau_I}, pI)$
	V	$(0, 0, 0, V) \rightarrow (Nr_D, 0, 0, -cV)$
Planes	TE	$(T, E, 0, 0) \rightarrow (r_D(N - T - E), -\frac{E}{\tau_E}, \frac{E}{\tau_E}, 0)$
	TI	$(T, 0, I, 0) \rightarrow (r_D(N - T - I), 0, -\frac{I}{\tau_I}, pI)$
	TV	$(T, 0, 0, V) \rightarrow (-\beta TV + r_D(N - T), 0, 0, -cV)$
	EI	$(0, E, I, 0) \rightarrow (r_D(N - E - I), -\frac{E}{\tau_E}, \frac{E}{\tau_E} - \frac{I}{\tau_I}, pI)$
	EV	$(0, E, 0, V) \rightarrow (r_D(N - E), -\frac{E}{\tau_E}, \frac{E}{\tau_E}, -cV)$
	IV	$(0, 0, I, V) \rightarrow (r_D(N - I), 0, -\frac{I}{\tau_I}, pI - cV)$
Hyperplanes	TEI	$(T, E, I, 0) \rightarrow (r_D(N - T - E - I), -\frac{E}{\tau_E}, \frac{E}{\tau_E} - \frac{I}{\tau_I}, pI)$
	TEV	$(T, E, 0, V) \rightarrow (-\beta TV + r_D(N - T - E), \beta TV - \frac{E}{\tau_E}, \frac{E}{\tau_E}, -cV)$
	TIV	$(T, 0, I, V) \rightarrow (-\beta TV + r_D(N - T - I), \beta TV, -\frac{I}{\tau_I}, pI - cV)$
	EIV	$(0, E, I, V) \rightarrow (r_D(N - E - I), -\frac{E}{\tau_E}, \frac{E}{\tau_E} - \frac{I}{\tau_I}, pI - cV)$

Table 1: Table to illustrate boundary behaviours

The cases listed in table [1] above point towards the interior of Ω when all the variables that do not make up the boundary being considered are non-negative. For example, when considering the TE plane, the I and V components must be greater than or equal to zero.

Without considering any of our biological constraints, all of the boundaries containing a T axis (TI and TV planes, and TEI, TEV, and TIV hyper-planes), as well as the V axis, meet the above requirement. This last statement is with the exception of the T axis, which is invariant. The E axis and the EV plane fit the requirement if $N \geq E$, the I axis and IV plane fit the requirement if $N \geq I$, and the EI plane and the EIV hyper-plane fit the requirement if $N \geq E + I$. Due to our biological constraint, $N = T + E + I + D$, N is in fact greater than the E, I, and E + I, making all the cases in the table above point towards the interior of Ω , as desired.

2.6. Well posedness. In order to secure the existence and uniqueness of solutions for a one dimensional ODE, $\frac{d}{dt}y = f(y)$, $f(y)$ must be continuous and $f'(y)$ must exist and be continuous. This can be extended to systems of differential equations, $\frac{d}{dt}F = F(x_1(t), x_2(t), \dots, x_n(t))$. The system must be continuous on an open set \mathcal{U} , the Jacobian matrix for F must be defined in \mathcal{U} , and the elements of the jacobian matrix must be continuous. In our case, $\mathcal{U} = \overset{\circ}{\Omega}$, the Jacobian exists and is continuous, see (10), over this region. Because $\mathcal{U} = \overset{\circ}{\Omega}$ does not account for the boundaries, the boundary behavior was analyzed to show that points on the boundary always go in towards the interior, see section ???. The only exception is the T-axis which it is invariant.

2.7. Local stability of equilibria.

Theorem 2.1. *The Disease Free Equilibrium is locally asymptotically stable when $\mathcal{R}_0 \leq 1$ and it is unstable when $\mathcal{R}_0 > 1$.*

Proof. Recall equilibrium points are locally stable when the eigenvalues of their Jacobian matrices have only negative real parts [50, 11].

We want to show that if $\mathcal{R}_0 \leq 1$ then the disease free equilibrium has asymptotic stability and if $\mathcal{R}_0 > 1$ then the disease free equilibrium is unstable. We must show that $\mathcal{R}_0 \leq 1$ produces only negative eigenvalues and that $\mathcal{R}_0 > 1$ produces at least one positive eigenvalue. Starting with the Jacobian matrix of the disease free equilibrium, (11), we compute the following:

First we obtain $\lambda I - J_{DFE}$:

$$(20) \quad \lambda I - J_{DFE} = \begin{pmatrix} \lambda + r_D & r_D & r_D & \beta N \\ 0 & \lambda + \frac{1}{\tau_E} & 0 & -\beta N \\ 0 & -\frac{1}{\tau_E} & \lambda + \frac{1}{\tau_I} & 0 \\ 0 & 0 & -p & \lambda + c \end{pmatrix}$$

Next we set the determinant of this matrix equal to zero:

$$(21) \quad \det(\lambda - J_{DFE}) = (\lambda + r_D) \left(\left(\lambda + \frac{1}{\tau_E} \right) \left(\lambda + \frac{1}{\tau_I} \right) (\lambda + c) - \frac{\beta N p}{\tau_E} \right) = 0$$

We notice that the term $\frac{\beta N p}{\tau_E}$ can easily be expressed in terms of \mathcal{R}_0 and we find that $\frac{\beta N p}{\tau_E} = \frac{c \mathcal{R}_0}{\tau_E \tau_I}$. Substituting in this term and simplifying equation 21, we obtain the following:

$$(22) \quad \det(\lambda I - J_{DFE}) = (\lambda + r_D) \left(\lambda^3 + \lambda^2 \left(\frac{1}{\tau_E} + \frac{1}{\tau_I} + c \right) + \lambda \left(\frac{1}{\tau_E \tau_I} + \frac{c}{\tau_E} + \frac{c}{\tau_I} \right) + \frac{c}{\tau_E \tau_I} \cdot (1 - \mathcal{R}_0) \right) = 0$$

We see that $\lambda = -r_D$ is a negative root so it only remains for us to consider the third degree polynomial. The coefficients of λ^3 , λ^2 , and λ are all always positive due to our assumptions about the parameters. The term corresponding to λ^0 is positive when $\mathcal{R}_0 \leq 1$ and negative when $\mathcal{R}_0 > 1$.

When $\mathcal{R}_0 \leq 1$ and all the signs of the coefficients of λ are positive, there are zero sign changes in the sequence of coefficients. By Descartes' Rule of signs [50, 13], there are zero real positive roots. So, when $\mathcal{R}_0 < 1$, all the real components of the eigenvalues are negative and we have local asymptotic stability, as desired. Similarly, when $\mathcal{R}_0 > 1$, there is one sign change in the sequence of coefficients, meaning we have exactly one positive root, giving us instability at the disease free equilibrium.

We can confirm that there are no roots with positive real parts when $\mathcal{R}_0 < 1$ through the Routh Hurwitz test. The Routh Hurwitz table for a third degree polynomial is constructed below,

$$\begin{array}{cc} a_3 & a_1 \\ a_2 & a_0 \\ \frac{a_2 a_1 - a_3 a_0}{a_2} & 0 \\ a_0 & 0 \end{array}$$

where a_3 is the coefficient of λ^3 , a_2 is the coefficient of λ^2 , and so on.

The Routh-Hurwitz test states that all the roots of the polynomial have real parts strictly less than zero if and only if all the elements in the leftmost column are nonzero and share the same sign [50, 14]. In our case, we need to show that a_3 , a_2 , $\frac{a_2 a_1 - a_3 a_0}{a_2}$, and a_0 are all positive.

We know that a_0, a_2 , and a_3 are all greater than zero because all of our parameters are positive and $\mathcal{R}_0 < 1$. It remains for us to look at $\frac{a_2 a_1 - a_3 a_0}{a_2}$. Since a_2 is positive, we only need to consider the numerator. We have:

$$(23) \quad a_2 a_1 - a_3 a_0 = \left(\frac{1}{\tau_E} + \frac{1}{\tau_I} + c \right) \left(\frac{1}{\tau_E \tau_I} + \frac{c}{\tau_E} + \frac{c}{\tau_I} \right) - \frac{c}{\tau_E \tau_I} \cdot (1 - \mathcal{R}_0)$$

$$(24) \quad = \frac{c \mathcal{R}_0}{\tau_E \tau_I} + \left(\frac{1}{\tau_E} + \frac{1}{\tau_I} + c \right) \left(\frac{1}{\tau_E \tau_I} + \frac{c}{\tau_E} + \frac{c}{\tau_I} \right) - \frac{c}{\tau_E \tau_I}$$

where the only negative term, $\frac{c}{\tau_E \tau_I}$, will cancel with one of the three positive $\frac{c}{\tau_E \tau_I}$ terms that are present when the $a_2 a_3$ term is expanded. So, we are left with a sum of positive values and $a_2 a_1 - a_3 a_0 > 0$, completing the Routh Hurwitz test and proving that the DFE is locally, asymptotically stable. \square

Theorem 2.2. *The Endemic Equilibrium is locally asymptotically stable when $\mathcal{R}_0 > 1$ and it is locally asymptotically unstable when $\mathcal{R}_0 \leq 1$.*

Proof. Next we will look for local stability for the endemic equilibrium when $\mathcal{R}_0 > 1$. We will denote this point by $(T, E, I, V) = (T^*, E^*, I^*, V^*)$. Our Jacobian at the endemic equilibrium (J_{EE}) after taking the difference from λI is as follows:

$$(25) \quad \lambda I - J_{EE} = \begin{pmatrix} \lambda + \beta V^* + r_D & r_D & r_D & \beta T^* \\ -\beta V^* & \lambda + \frac{1}{\tau_E} & 0 & -\beta T^* \\ 0 & -\frac{1}{\tau_E} & \lambda + \frac{1}{\tau_I} & 0 \\ 0 & 0 & -p & \lambda + c \end{pmatrix}$$

From this we can calculate the characteristic polynomial of J_{EE} .

$$(26) \quad \det(\lambda I - J_{EE}) = (\lambda + \beta V^* + r_D) \begin{vmatrix} \lambda + \frac{1}{\tau_E} & 0 & -\beta T^* \\ -\frac{1}{\tau_E} & \lambda + \frac{1}{\tau_I} & 0 \\ 0 & -p & \lambda + c \end{vmatrix} + \beta V^* \begin{vmatrix} r_D & r_D & \beta T^* \\ -\frac{1}{\tau_E} & \lambda + \frac{1}{\tau_I} & 0 \\ 0 & -p & \lambda + c \end{vmatrix}$$

$$(27) \quad = (\lambda + \beta V^* + r_D) \left(\left(\lambda + \frac{1}{\tau_E} \right) \left(\lambda + \frac{1}{\tau_I} \right) (\lambda + c) - \frac{\beta T^* p}{\tau_E} \right) + \beta V^* \left(r_D \left(\lambda + \frac{1}{\tau_I} \right) (\lambda + c) + \frac{1}{\tau_E} (r_D (\lambda + c) + p \beta T^*) \right)$$

This term is expanded and simplified because it cannot be factored. T^* is replaced by its equivalent form, $\frac{c}{p\beta\tau_I}$, to aid with the simplification. We are left with a characteristic polynomial with the coefficients listed below. The term corresponding to λ^4 is named a_4 , the term with λ^3 is named a_3 , and so forth.

$$\begin{aligned}
 a_0 &= \frac{cr_D}{\tau_I} + \frac{cr_D}{\tau_E} + \frac{c}{\tau_E\tau_I} \\
 a_1 &= \frac{2r_d}{\tau_E} + \frac{2r_D}{\tau_I} + cr_D + \frac{\beta V^* c}{\tau_I} + \frac{\beta V^* c}{\tau_E} + \frac{\beta V^*}{\tau_E\tau_I} + \frac{r_D}{\tau_E\tau_I} \\
 a_2 &= \frac{c}{\tau_I} + \frac{c}{\tau_E} + \frac{1}{\tau_E\tau_I} + r_D + \beta V^* c + \frac{\beta V^*}{\tau_E} + \frac{\beta V^*}{\tau_I} + r_{DC} + \frac{r_D}{\tau_E} + \frac{r_D}{\tau_I} \\
 a_3 &= c + \frac{1}{\tau_E} + \frac{1}{\tau_I} + \beta V^* + r_D \\
 a_4 &= 1
 \end{aligned}$$

With these coefficients we can use the Routh Hurwitz test to show that when $\mathcal{R}_0 > 1$ we have only negative real roots. The Routh Hurwitz table for a fourth degree polynomial is constructed below.

$$\begin{array}{ccc}
 a_4 & a_2 & a_0 \\
 a_3 & a_1 & 0 \\
 b_1 = \frac{a_3 a_2 - a_4 a_1}{a_3} & a_0 & 0 \\
 \frac{a_1 b_1 - a_3 a_0}{b_1} & 0 & 0 \\
 a_0 & 0 & 0
 \end{array}$$

We thus need to verify that the most left column has non-zero elements with the same sign. Since the coefficients of the characteristic polynomial are positive, we must show that $a_4, a_3, a_0, b_1 = \frac{a_3 a_2 - a_4 a_1}{a_3}$ and $\frac{a_1 b_1 - a_3 a_0}{b_1}$ are all greater than zero. Note that because $\mathcal{R}_0 > 1, T^*, E^*, I^*$ and V^* are all positive values. Also, our biological constraints give us the assumption that all of the parameters are greater than zero.

Starting with the least complex terms we have that: $a_4 = 1 > 0$.

So we also have:

$$a_3 = c + \frac{1}{\tau_E} + \frac{1}{\tau_I} + \beta V^* + r_D > 0$$

$$a_0 = \frac{cr_D}{\tau_I} + \frac{cr_D}{\tau_E} + \frac{c}{\tau_E \tau_I} > 0$$

Next we look at b_1 . We know that the denominator, a_3 , is positive from above so it only remains to show that the numerator, $a_3a_2 - a_4a_1$ is positive. When $a_3a_2 - a_4a_1$ is expanded all of the negative terms from a_4a_1 cancel with positive terms from a_3a_2 and we are left with the following sum of positive terms:

$$\begin{aligned} a_3a_2 - a_4a_1 &= \frac{c^2}{\tau_I} + \frac{c^2}{\tau_E} + \frac{3c}{\tau_I \tau_E} + c^2 \beta V^* + \frac{2c\beta V^*}{\tau_E} + \frac{2c\beta V^*}{\tau_I} + r_D c^2 + \frac{2cr_D}{\tau_I} + \frac{c}{\tau_I^2} \\ &+ \frac{1}{\tau_I^2 \tau_E} + \frac{2\beta V^*}{\tau_E \tau_I} + \frac{\beta V^*}{\tau_I^2} + \frac{r_D}{\tau_I^2} + \frac{c}{\tau_E^2} + \frac{1}{\tau_I \tau_E^2} + \frac{2r_D c}{\tau_E} + \frac{r_D}{\tau_E^2} + \frac{2r_D}{\tau_I \tau_E} + r_D \beta V^* \\ &+ c(\beta V^*)^2 + \frac{(\beta V^*)^2}{\tau_E} + \frac{(\beta V^*)^2}{\tau_I} + 2\beta V^* r_D c + \frac{2\beta V^* r_D}{\tau_E} + \frac{2\beta V^* r_D}{\tau_I} + r_D^2 c \\ &+ \frac{r_D^2}{\tau_E} + \frac{r_D^2}{\tau_I} > 0 \end{aligned}$$

Finally we look at $\frac{a_1 b_1 - a_3 a_0}{b_1}$. Since $b_1 > 0$ we can look solely at the numerator, $a_1 b_1 - a_3 a_0$. Through some algebraic manipulation we obtain the following:

$$a_1 b_1 - a_3 a_0 = a_1 \left(\frac{a_3 a_2 - a_4 a_1}{a_3} \right) - a_3 a_0 = a_1 a_2 - \frac{a_1^2}{a_3} - a_3 a_0$$

Since $a_3 > 0$, we multiply through by a_3 :

$$a_1 a_2 a_3 - a_1^2 - a_3 a_0^2 = a_1 (a_2 a_3 - a_1) - a_3^2 a_0$$

This arrangement of terms lets us utilize the term $a_2 a_3 - a_1$ that we used to show $b_1 > 0$. Because $a_1 > 0$ and $a_2 a_3 - a_1 > 0$, their product is positive. When this product is expanded and written with specific grouping we get 203 positive terms. When $a_3^2 a_0$ is expanded and the negative is distributed and written with specific grouping we get 45 negative terms. 36 of these negative terms correspond directly with positive terms so they cancel, leaving us with nine negative terms. It remains for us to show that the sum of positive terms that did not cancel is larger than the sum of the nine remaining negative terms. Showing this will guarantee that all

the terms in the leftmost column of the Routh-Hurwitz table are positive. We need to show that the positive terms are greater than the negative terms, so instead of showing that $a_1b_1 - a_3a_0 > 0$, we want to show that the remaining positive terms minus the remaining negative terms is strictly greater than 0.

We are now left with exactly 203 - 45 terms because some negative terms only canceled with part of the corresponding positive part. For example, the positive term $\frac{4c\beta V^* r_D}{\tau_E^2}$ cancels out the negative term $\frac{2c\beta V^* r_D}{\tau_E^2}$. This does not leave us with zero but with the positive term $\frac{2c\beta V^* r_D}{\tau_E^2}$. This occurs several times and we end up with 181 remaining positive terms. Let us denote the sequence of the i remaining positive terms with \mathcal{P} and the j remaining negative terms with \mathcal{N} . We will show that:

$$(28) \quad \sum_1^{181} \mathcal{P}_i > \sum_1^9 \mathcal{N}_j$$

Because of the Arithmetic Geometric Mean, we know that

$$(29) \quad \frac{1}{181} \cdot \sum_1^{181} \mathcal{P}_i > \left(\prod_1^{181} \mathcal{P}_i \right)^{\frac{1}{181}}$$

Stringing 28 and 29 together we find that it is enough to show the following:

$$(30) \quad 181 \cdot \left(\prod_1^{181} \mathcal{P}_i \right)^{\frac{1}{181}} > \sum_1^9 \mathcal{N}_j$$

Substituting our actual terms to 30 we obtain:

$$181 \cdot \left(\frac{3^4 \cdot 2^{97} \cdot c^{171} (\beta V^*)^{182} r_D^{214}}{\tau_E^{208} \tau_I^{224}} \right)^{\frac{1}{181}} > \frac{c}{\tau_E \tau_I} \left(c^2 + \frac{2c}{\tau_I} + \frac{2c}{\tau_E} + 2\beta V^* c + \frac{1}{\tau_I^2} + \frac{2}{\tau_E \tau_I} + \frac{2\beta V^*}{\tau_I} + \frac{1}{\tau_E^2} + \frac{2\beta V^*}{\tau_E} \right)$$

Which can also be written as the following when we divide out $\frac{c}{\tau_E \tau_I}$:

$$181 \cdot \left(\frac{3^4 \cdot 2^{97} (\beta V^*)^{182} r_D^{214}}{c^{10} \tau_E^{27} \tau_I^{43}} \right)^{\frac{1}{181}} > c^2 + \frac{2c}{\tau_I} + \frac{2c}{\tau_E} + 2\beta V^* c + \frac{1}{\tau_I^2} + \frac{2}{\tau_E \tau_I} + \frac{2\beta V^*}{\tau_I} + \frac{1}{\tau_E^2} + \frac{2\beta V^*}{\tau_E}$$

Next we place some constraints on $c, \beta V^*, \frac{1}{\tau_E}, \frac{1}{\tau_I}$, and r_D . In order to make this less complicated we split the above inequality into nine separate pieces. We compare one ninth of the left-hand side to each individual term on the right. Our new inequalities are as follows:

$$\begin{aligned} \frac{181}{9} \cdot \left(\frac{\cdot 3^4 \cdot 2^{97} (\beta V^*)^{182} r_D^{214}}{c^{10} \tau_E^{27} \tau_I^{43}} \right)^{\frac{1}{181}} &> c^2 \\ \frac{181}{9} \cdot \left(\frac{\cdot 3^4 \cdot 2^{97} (\beta V^*)^{182} r_D^{214}}{c^{10} \tau_E^{27} \tau_I^{43}} \right)^{\frac{1}{181}} &> \frac{2c}{\tau_I} \\ &\vdots \\ \frac{181}{9} \cdot \left(\frac{\cdot 3^4 \cdot 2^{97} (\beta V^*)^{182} r_D^{214}}{c^{10} \tau_E^{27} \tau_I^{43}} \right)^{\frac{1}{181}} &> \frac{2\beta V^*}{\tau_E} \end{aligned}$$

Looking at just the greater component, we separate the numerical components and the parameter components.

$$\frac{181}{9} \cdot \left(\frac{\cdot 3^4 \cdot 2^{97} (\beta V^*)^{182} r_D^{214}}{c^{10} \tau_E^{27} \tau_I^{43}} \right)^{\frac{1}{181}} = \frac{181 \cdot 3^{\frac{4}{181}} \cdot 2^{\frac{97}{181}}}{9} \cdot \left(\frac{(\beta V^*)^{182} r_D^{214}}{c^{10} \tau_E^{27} \tau_I^{43}} \right)^{\frac{1}{181}}$$

We now place the assumption that $\left(\frac{(\beta V^*)^{182} r_D^{214}}{c^{10} \tau_E^{27} \tau_I^{43}} \right) > 1$. We will return to this assumption after we have set constraints on $c, \beta V^*, \frac{1}{\tau_E}$ and $\frac{1}{\tau_I}$ to set constraints for r_D . Now it is enough to show that:

$$\begin{aligned} \frac{181 \cdot 3^{\frac{4}{181}} \cdot 2^{\frac{97}{181}}}{9} &> c^2 \\ \frac{181 \cdot 3^{\frac{4}{181}} \cdot 2^{\frac{97}{181}}}{9} &> \frac{2c}{\tau_I} \\ &\vdots \\ \frac{181 \cdot 3^{\frac{4}{181}} \cdot 2^{\frac{97}{181}}}{9} &> \frac{2\beta V^*}{\tau_E} \end{aligned}$$

Looking specifically at the first inequality listed, we can obtain an upper bound for c .

$$(31) \quad c < \sqrt{\frac{181 \cdot 3^{\frac{4}{181}} \cdot 2^{\frac{97}{181}}}{9}} \approx 5.47$$

Next we follow a similar approach to acquire upper bounds for $\frac{1}{\tau_E}$, $\frac{1}{\tau_I}$ and βV^* , plugging the upper bound in for c where necessary. We obtain the same upper bound for all three.

$$(32) \quad \frac{1}{\tau_E}, \frac{1}{\tau_I}, \beta V^* < \frac{c}{2} = \frac{1}{2} \cdot \sqrt{\frac{181 \cdot 3^{\frac{4}{181}} \cdot 2^{\frac{97}{181}}}{9}} \approx 2.73$$

When we plug all these bounds in for the remaining five inequalities, all the inequalities are satisfied, ensuring that none of the bounds lead to any contradictions. One example is shown below.

$$\frac{181 \cdot 3^{\frac{4}{181}} \cdot 2^{\frac{97}{181}}}{9} > \frac{1}{\tau_I^2} = \left(\frac{1}{2} \cdot \sqrt{\frac{181 \cdot 3^{\frac{4}{181}} \cdot 2^{\frac{97}{181}}}{9}} \right)^2 = \frac{1}{4} \cdot \frac{181 \cdot 3^{\frac{4}{181}} \cdot 2^{\frac{97}{181}}}{9}$$

Finally, we return to the term we earlier let be greater than one, $\frac{(\beta V^*)^{182} r_D^{214}}{c^{10} \tau_E^{27} \tau_I^{43}} > 1$.

Plugging in the bounds we have acquired for c , $\frac{1}{\tau_E}$, $\frac{1}{\tau_I}$ and βV^* , we will find a lower bound for r_D . after combining the terms with the same bounds, rearranging to isolate r_D , and plugging in with the values, we obtain the following:

$$(33) \quad r_D > \frac{c^{\frac{10}{214}}}{(\beta V^*)^{\frac{252}{214}}} = \left(4^{126} \cdot \left(\frac{9}{181 \cdot 3^{\frac{4}{181}} \cdot 2^{\frac{97}{181}}} \right)^{121} \right)^{\frac{1}{214}} \approx .331$$

So, all together we can guarantee local stability when $c < 5.47$, βV^* , $\frac{1}{\tau_E}$, $\frac{1}{\tau_I} < 2.73$, and $r_D > .331$. Let us recall that all these parameters interact with one another. We can still have local stability if one of these parameters exceeds its bound if the quantities of the other parameters are altered from their bounds appropriately. Also, keep in mind that we are showing 30 while we actually only require 28, giving us even more freedom on these parameter bounds. \square

2.8. Global stability of equilibria. Lyapunov functions are powerful tools for determining the global stability of equilibrium points. Let $U \subset \mathbb{R}^4$ be a neighborhood of 0, then a Lyapunov function, denoted as $L(x)$ is a real-valued function that is decreasing across the entire vector field, f , that is defined by the ODE system. Since $L(x)$ is decreasing along f , intuitively we would expect that the lowest point of $L(x)$ should be a stable equilibrium point. Since Lyapunov functions need to be decreasing over time, we know that $\dot{L}(\mathbf{X}) = \nabla(L(\mathbf{X})) \cdot \dot{\mathbf{X}}$ must be less than or equal to 0. There are three circumstances that could arise from $L(\mathbf{X})$ and $\dot{L}(\mathbf{X})$.

(1) If

- $L(\mathbf{X}) \geq 0$ for all $\mathbf{X} \in U$
- $L(\mathbf{X}) = 0$ if and only if $\mathbf{X} = \mathbf{0}$
- $\dot{L}(\mathbf{X}) \leq 0$ for all $\mathbf{X} \in U$

then $\mathbf{X} = \mathbf{0}$ is a locally stable equilibrium point.

(2) If

- $L(\mathbf{X}) \geq 0$ for all $\mathbf{X} \in U$
- $L(\mathbf{X}) = 0$ if and only if $\mathbf{X} = \mathbf{0}$
- $\dot{L}(\mathbf{0}) = 0$ and $\dot{L}(\mathbf{X}) < 0$ for all $\mathbf{X} \neq \mathbf{0}$ contained in U

then $\mathbf{X} = \mathbf{0}$ is locally asymptotically stable equilibrium point.

(3) If

- $L(\mathbf{0}) = 0$ and there exists some sequence of values \mathbf{X}_n where $L(\mathbf{X}_n) < 0$ for all n and $\mathbf{X}_n \rightarrow \mathbf{0}$
- $\dot{L}(\mathbf{0}) = 0$ and $\dot{L}(\mathbf{X}) < 0$ for all $\mathbf{X} \neq \mathbf{0}$ and in U

then $\mathbf{X} = \mathbf{0}$ is an unstable equilibrium point.

The Lyapunov function also provides us with a method of finding when equilibrium points are globally asymptotically stable. Let K be the largest invariant set in \mathbb{R}^4 such that $\dot{L}(\mathbf{X}) = 0$. This can be thought of as the set of all points (T, E, I, V) that remain within a set K at any time. If K consists of a single point, \mathbf{X}^* , then \mathbf{X}^* is an equilibrium point that is globally asymptotically stable, this is known as LaSalle's Invariance Principle [31]. Let us now look to our system of equations.

Theorem 2.3. *Let $R_0 < 1$, and consider the Disease-Free Equilibrium. This is globally asymptotically stable with respect to initial conditions in Ω if $\frac{2N}{T} + \frac{p}{r_D} <$*

$$2 + \frac{1}{\tau_I r_D} \text{ and } \frac{\mathcal{R}_0}{\tau_I p} < 1.$$

Proof. Let us consider the function

$$(34) \quad L(\mathbf{X}) = \int_N^T 1 - \frac{N}{x} dx + E + I + V$$

Notice that (34) is a nonnegative function for any $\mathbf{X} \in \Omega$. Moreover, $L(\mathbf{X}) = 0$ if and only if $\mathbf{X} = X_{DFE} = (N, 0, 0, 0)$.

Finally,

$$\begin{aligned} \dot{L}(\mathbf{X}) &= \left(1 - \frac{N}{T}\right)\dot{T} + \dot{E} + \dot{I} + \dot{V} \\ &= \left(1 - \frac{N}{T}\right)(-\beta TV - r_D(N - T - E - I)) + \left(\beta TV - \frac{E}{\tau_E}\right) + \left(\frac{E}{\tau_E} - \frac{I}{\tau_I}\right) + (pI - cV) \\ &= r_D(N - T)\left(1 - \frac{N}{T}\right) + r_D\left(1 - \frac{N}{T}\right)(-E - I) + \beta NV - \frac{I}{\tau_I} + pI - cV \\ &\leq r_D(N - T)\left(1 - \frac{N}{T}\right) + r_D\left(1 - \frac{N}{T}\right)(-2N) + \beta NV + I\left(p - \frac{1}{\tau_I}\right) - cV \\ &= r_D(N - T)\left(1 - \frac{N}{T}\right) + r_D\left(\frac{N}{T} - 1\right)(2N) + V(\beta N - c) + I\left(p - \frac{1}{\tau_I}\right) \\ &\leq r_D(N - T)\left(1 - \frac{N}{T}\right) + r_D\left(\frac{N}{T} - 1\right)(2N) + V(\beta N - c) + N\left(p - \frac{1}{\tau_I}\right) \\ &= r_D(N - T)\left(1 - \frac{N}{T}\right) + N\left(\frac{2r_D N}{T} - 2r_D + p - \frac{1}{\tau_I}\right) + V(\beta N - c) \\ &= r_D(N - T)\left(1 - \frac{N}{T}\right) + N\left(\frac{2r_D N}{T} - 2r_D + p - (2r_D \frac{1}{\tau_I})\right) + Vc\left(\frac{\mathcal{R}_0}{\tau_I p} - 1\right) \end{aligned}$$

Because of our biological conditions, $N > T + E + I$ which allows for the substitutions made above. Also, it ensures that our first term, $r_D(N - T)\left(1 - \frac{N}{T}\right)$, is negative. The following two terms will be negative from our conditions set at the beginning of this proof. So, $L(\mathbf{X}) < 0$, giving us global stability about the DFE. \square

Theorem 2.4. *Let $X^* = (T^*, E^*, I^*, V^*)$ be a positive steady state of the system (1-4). Then X^* is globally asymptotically stable with respect to initial conditions in $\overset{\circ}{\Omega}$ if $T^* < T, E^* < E, I^* < I, V^* < V$ and $V^* < 4V$, and $pI < cV$.*

Proof. Let us consider the system (1)-(4), we will prove the existence of a Lyapunov function. Let us notice that any steady state holds the following steady state equations:

$$(35) \quad \beta T^* V^* = r_D(N - T^* - E^* - I^*) = \frac{E^*}{\tau_E} = \frac{I^*}{\tau_I}$$

$$(36) \quad pI^* = cV^*$$

We define the function

$$(37) \quad L(\mathbf{X}) = \int_{T^*}^T 1 - \frac{T^*}{x} dx + \int_{E^*}^E 1 - \frac{E^*}{x} dx + \int_{I^*}^I 1 - \frac{I^*}{x} dx + \alpha \int_{V^*}^V 1 - \frac{V^*}{x} dx$$

where α is a positive constant, defined later. Notice that for any $X \in \Omega$ is such that $V(X) \geq 0$ where $V(X) = 0$ if and only if $X = X^*$. Furthermore, notice that

$$\begin{aligned} L(\dot{\mathbf{X}}) &= \nabla(L(\mathbf{X})) \cdot \dot{\mathbf{X}} = \left(1 - \frac{T^*}{T}\right) \dot{T} + \left(1 - \frac{E^*}{E}\right) \dot{E} + \left(1 - \frac{I^*}{I}\right) \dot{I} + \alpha \left(1 - \frac{V^*}{V}\right) \dot{V} \\ &= \left(1 - \frac{T^*}{T}\right) (-\beta TV + r_D(N - T - E - I)) + \left(1 - \frac{E^*}{E}\right) (\beta TV - \frac{E}{\tau_E}) \\ &\quad + \left(1 - \frac{I^*}{I}\right) \left(\frac{E}{\tau_E} - \frac{I}{\tau_I}\right) \alpha \left(1 - \frac{V^*}{V}\right) (pI - cV) \end{aligned}$$

Now we strategically add terms that sum to zero and algebraically manipulate the above.

$$\begin{aligned} &= \left(1 - \frac{T^*}{T}\right) \left(-\beta TV + r_D(N - T - E - I - N + T^* + E^* + I^*) + r_D(N - T^* - E^* - I^*)\right) \\ &\quad + \beta TV - \frac{E}{\tau_E} - \frac{\beta TVE^*}{E} + \frac{E^*}{\tau_E} + \frac{E}{\tau_E} - \frac{I}{\tau_I} - \frac{I^*E}{I\tau_E} + \frac{I^*}{\tau_I} + \alpha \left(1 - \frac{V^*}{V}\right) (pI - cV) \\ &= \left(1 - \frac{T^*}{T}\right) r_D(T^* - T + E^* - E + I^* - I) + \left(1 - \frac{T^*}{T}\right) (-\beta TV) \\ &\quad + \left(1 - \frac{T^*}{T}\right) r_D(N - T^* - E^* - I^*) + \beta TV - \beta TV \left(\frac{E^*}{E}\right) + \frac{E^*}{\tau_E} - \frac{I}{\tau_I} - \frac{I^*E}{I\tau_I} + \frac{I^*}{\tau_I} + \\ &\quad \alpha \left(1 - \frac{V^*}{V}\right) (pI - cV) \end{aligned}$$

$$\begin{aligned}
&= \left(1 - \frac{T^*}{T}\right) r_D(T^* - T + E^* - E + I^* - I) + \beta T^* V + \beta T^* V^* - \frac{T^*}{T} \beta T^* V^* - \frac{E^*}{T^* V^* \tau_E} \\
&\quad \cdot \frac{TVE^*}{E} + \frac{E^*}{\tau_E} - \frac{I^* E}{\tau_E I} - \frac{I}{\tau_I} + \frac{I^*}{\tau_I} + \alpha \left(1 - \frac{V^*}{V}\right) (pI - cV) \\
&= \left(1 - \frac{T^*}{T}\right) r_D(T^* - T + E^* - E + I^* - I) + \beta T^* V + \frac{I^*}{\tau_I} - \frac{T^* I^*}{T \tau_I} + \frac{TVE^* I^*}{T^* V^* E \tau_I} + \frac{I^*}{\tau_I} \\
&\quad - \frac{I^* E}{\tau_E I} - \frac{II^*}{\tau_I I^*} + \frac{I^*}{\tau_I} + \alpha \left(1 - \frac{V^*}{V}\right) (pI - cV) \\
&= \left(1 - \frac{T^*}{T}\right) r_D(T^* - T + E^* - E + I^* - I) + \frac{V I^*}{V^* \tau_I} + \frac{I^*}{\tau_I} - \frac{T^* I^*}{T \tau_I} - \left(\frac{TVE^*}{T^* V^* E}\right) \frac{I^*}{\tau_I} + \frac{I^*}{\tau_I} \\
&\quad - \left(\frac{I^* E}{IE^*}\right) \frac{I^*}{\tau_I} - \frac{I I^*}{I^* \tau_I} + \frac{I^*}{\tau_I} + \alpha \left(1 - \frac{V^*}{V}\right) (pI - cV) \\
&= \left(1 - \frac{T^*}{T}\right) r_D(T^* - T + E^* - E + I^* - I) + \frac{I^*}{\tau_I} \left(\frac{V}{V^*} + 1 - \frac{T^*}{T} - \frac{TVE^*}{T^* V^* E} + 1 - \frac{I^* E}{IE^*} - \frac{I}{I^*} + 1\right) + \\
&\quad \alpha \left(1 - \frac{V^*}{V}\right) (pI - cV) \\
&= \left(1 - \frac{T^*}{T}\right) r_D(T^* - T + E^* - E + I^* - I) + \frac{I^*}{\tau_I} \left(1 - \frac{T^*}{T} - \frac{TVE^*}{T^* V^* E} - \frac{I^* E}{IE^*} - \frac{I}{I^*}\right) + \frac{I^*}{\tau_I} \left(\frac{V}{V^*} + 2\right) \\
&\quad \alpha \left(1 - \frac{V^*}{V}\right) (pI - cV)
\end{aligned}$$

We know that the first term, $\left(1 - \frac{T^*}{T}\right) r_D(T^* - T + E^* - E + I^* - I)$ is negative from our conditions. Looking at the second term, we want the magnitude of the negative terms to be greater than the positive terms. As in the local stability, we will utilize the Arithmetic Geometric Mean. Since there are 4 negative terms we know the following:

$$(38) \quad \sum_{i=1}^4 \mathcal{N}_i \geq 4 \left(\prod_{i=1}^4 \mathcal{N}_i \right)^{\frac{1}{4}}$$

So, it is enough to show that four times the fourth root of the product of the negative terms is greater than 1.

$$(39) \quad 4 \left(\prod_{i=1}^4 \mathcal{N}_i \right)^{\frac{1}{4}} = 4 \left(\frac{T^*}{T} \cdot \frac{TV E^*}{T^* V^* E} \cdot \frac{I^* E}{I E^*} \cdot \frac{I}{I^*} \right)^{\frac{1}{4}} = 4 \left(\frac{V}{V^*} \right)^{\frac{1}{4}}$$

Setting this result greater than 1 and rearranging our terms, we obtain the inequality $V > \frac{1}{4}V^*$, which follows from our hypotheses. So, this term is negative.

We are now left with two terms, $\frac{I^*}{\tau_I} \left(\frac{V}{V^*} + 2 \right)$ and $\alpha \left(1 - \frac{V^*}{V} \right) (pI - cV)$. Due to our conditions, we know that the term attached to α is negative. So, we define α so that we ensure the negative term overpowers the only remaining positive one. We define α as:

$$(40) \quad \alpha = k \cdot \frac{I^*}{\tau_I} \left(\frac{V}{V^*} + 2 \right)$$

where k is some constant that is larger than one when multiplied with $\left(1 - \frac{V^*}{V} \right) (pI - cV)$. \square

3. STOCHASTIC MODEL

In Discrete-Time Markov Chains, time is considered to be a discrete variable that can take on the values $t_0 + n\Delta t$ for $n \in \mathbb{N}$ and some initial time t_0 . Thus, in order to make use of Discrete-Time Markov Chains, one must be able to reasonably assume that Δt can be chosen to be small enough so that at most one event occurs during Δt [4, 32]. On the other hand in Continuous-Time Markov Chains, $t \in [0, \infty)$, which frees us from needing to make such an assumption. However, Continuous-Time Markov Chains can be very computationally expensive, as they require generating exponential random variables that dictate how long a cell or person stays in a given state within the model [25, 45]. Additionally, given a population of size N , $N + 1$ Kolmogorov's differential equations would be needed for one of the most basic epidemiological models, an SIS model, in the case of Continuous-Time Markov Chains [28]. Previous biological models have produced Discrete-Time Markov Chains that are more efficient than Continuous-Time models and produce stochastically identical

results in the case of biochemical network modeling [45] and genetic regulatory network modeling [26]. However, these biological situations may lend themselves more easily to DTMC models due to having only one independent variable.

Continuous-Time Markov Chains are a popular and well-studied model for the spread of infectious diseases [4, 6, 17, 52]. We have chosen instead to focus on a DTMC model in order to better study methods for using this type of model to predict the spread of infectious diseases and to develop a more computationally efficient model than ones used in the past.

We have chosen to focus on Discrete Homogenous-Time Markov Chains for the stochastic modeling of within-host dynamics of influenza. In this type of model, the classes a cell can be in and time are discrete variables. In our case, a cell may be a target, exposed, infectious, or dead cell in any of the time values $\{t_0, t_0 + \Delta t, t_0 + 2\Delta t, \dots\}$. The homogeneous-time aspect of our model indicates that we are assuming that the probability of transitioning between the classes of our model does not depend on time. We will assume that we have a fixed number of cells that may fall in the classes of target cell, exposed cell, infectious cell, or dead cell. The random variables in the stochastic model will be denoted in calligraphic letters to avoid confusion with the non-random variables in the deterministic model. If we let N be the total number of cells, \mathcal{T} be the random variable representing the number of target cells, \mathcal{E} be the random variable representing the number of exposed cells, \mathcal{I} be the random variable representing the number of infectious cells, and \mathcal{D} be the random variable representing number of dead cells, then we have the dynamic states equation

$$N = \mathcal{T} + \mathcal{E} + \mathcal{I} + \mathcal{D}.$$

Within this model, there are five events that could occur. Some of these events also affect the amount of virus present, represented by the random variable \mathcal{V} . These events and the probability of them occurring are summarized in the below table. Notice that the transition probabilities are given by the transition rates seen in the deterministic ODE model multiplied by Δt .

Notice also that since N is a constant and due to the biological constraint $N = \mathcal{T} + \mathcal{E} + \mathcal{I} + \mathcal{D}$, we have one dependent variable and three independent variables. We choose our dependent variable to be \mathcal{D} , leaving our independent variables as \mathcal{T} , \mathcal{E} , and \mathcal{I} . This set-up is a multivariate stochastic process $\{(\mathcal{T}(t), \mathcal{E}(t), \mathcal{I}(t))|_{t=0}^{\infty}\}$, that is

Transition Events and Their Probabilities

Event	Event Description	Transitions	Probability of Event Occurring between time t and $t + \Delta t$
1	Target cell becomes exposed to the viron	$\mathcal{T} \rightarrow \mathcal{T} - 1,$ $\mathcal{E} \rightarrow \mathcal{E} + 1$	$\beta\mathcal{T}\mathcal{V}\Delta t$
2	Exposed cell becomes infectious	$\mathcal{E} \rightarrow \mathcal{E} - 1,$ $\mathcal{I} \rightarrow \mathcal{I} + 1$	$\frac{\mathcal{E}}{\tau_E}\Delta t$
3	Infectious cell dies	$\mathcal{I} \rightarrow \mathcal{I} - 1,$ $\mathcal{D} \rightarrow \mathcal{D} + 1$	$\frac{\mathcal{I}}{\tau_I}\Delta t$
4	Cellular restoration	$\mathcal{D} \rightarrow \mathcal{D} - 1,$ $\mathcal{T} \rightarrow \mathcal{T} + 1$	$r_D\mathcal{D}\Delta t$
5	No change	No transitions	$1 - \left(\beta\mathcal{T}\mathcal{V} + \frac{\mathcal{E}}{\tau_E} + \frac{\mathcal{I}}{\tau_I} + r_D\mathcal{D} \right) \Delta t$

Table 2: Table containing all transitions and their probabilities in the stochastic model.

time-homogeneous and should satisfy the Markov property, discussed below. Thus, we may write our joint probability density function as

$$(41) \quad P_{t,e,i}(t) := \Pr[(\mathcal{T}(t), \mathcal{E}(t), \mathcal{I}(t)) = (t, e, i)]$$

where $t, e, i \in \{0, 1, 2, \dots, M\}$. We define M to be the total number of live cells which is bound by the total population size N such that $\mathcal{T}(t) + \mathcal{E}(t) + \mathcal{I}(t) = M \leq N$, this means that the sum of $\mathcal{T}(t), \mathcal{E}(t), \mathcal{I}(t)$ can never exceed the size of the entire population. We can assume that Δt can be sufficiently small such that at most one change in state occurs during the time interval Δt . The probability of transition from the state (t, e, i) to the state $(t+k, e+j, i+l)$ is defined (using the notation in [3] and [32]) by

$$P_{t+k,e+j,i+l}(\Delta t) = \Pr[(\Delta\mathcal{T}, \Delta\mathcal{E}, \Delta\mathcal{I}) = (k, j, l) \mid (\mathcal{T}(t), \mathcal{E}(t), \mathcal{I}(t)) = (t, e, i)]$$

where

$$\Delta\mathcal{T} = \mathcal{T}(t + \Delta t), \quad \Delta\mathcal{E} = \mathcal{E}(t + \Delta t), \quad \text{and} \quad \Delta\mathcal{I} = \mathcal{I}(t + \Delta t)$$

We assume that the joint probability density function (41) holds the Markov Property.

Definition 3.1. The **Markov Property** holds that the state at time $t + \Delta t$ is dependent only on the state at time t and is independent of all previous times. If X_t is a vector describing our state at time t , then the Markov Property may be written as

$$\Pr(X_{t+\Delta t} = b | X_t, X_{t-\Delta t}, \dots, X_{\Delta t}, X_0) = \Pr(X_{t+\Delta t} = b | X_t).$$

If the Markov Property holds, then the values of $\mathcal{T}(t + \Delta t)$, $\mathcal{E}(t + \Delta t)$, $\mathcal{I}(t + \Delta t)$, and $\mathcal{D}(t + \Delta t)$ depend only on the values of $\mathcal{T}(t)$, $\mathcal{E}(t)$, and $\mathcal{I}(t)$.

It is reasonable to assume that our model holds the Markov Property because we would not expect the probability that transition from a current disease state to a new disease state to depend on past disease states. The only factors that should affect the transition from the current disease state are how many virions, target cells, exposed cell, infectious cells, and dead cells there are at each moment; all of which are encompassed in the current disease state. The Markov Property is important for understanding a component of our stochastic model, the transition matrix. The transition matrix is a matrix that governs how values change from one time to the next. The Markov Property allows us to make use of the transition matrix in the following manner.

Denote the transition matrix as \mathcal{M} and the random vector of values of describing the state at time t as $X(t)$. Then,

$$\begin{aligned} X(t_0 + \Delta t) &= \mathcal{M} \cdot X(t_0) \\ X(t_0 + 2\Delta t) &= \mathcal{M} \cdot X(t_0 + \Delta t) = \mathcal{M}^2 \cdot X(t_0) \\ &\vdots \\ X(t_0 + n\Delta t) &= \mathcal{M} \cdot X(t_0 + (n-1)\Delta t) = \mathcal{M}^n \cdot X(t_0). \end{aligned}$$

We give a more formal definition of the transition matrix.

Definition 3.2. The **transition matrix** of the Discrete Time Markov Chain $\{X_n\}_{n=0}^{\infty}$ with state space $\{1, 2, \dots\}$ and one-step transition probabilities, $\{p_{ab}\}_{a,b=1}^{\infty}$, is denoted

as $\mathcal{M} = (p_{ab})$, where

$$\mathcal{M} = \begin{bmatrix} p_{00} & p_{01} & p_{02} & \cdots \\ p_{10} & p_{11} & p_{12} & \cdots \\ p_{20} & p_{21} & p_{22} & \cdots \\ \vdots & \vdots & \vdots & \ddots \end{bmatrix}.$$

In this case, p_{ab} is the probability of transitioning from state a at time t to state b at time $t + \Delta t$ and $\sum_b p_{ab} = 1$ [2, 47].

Discrete Markov Chains are most commonly used when the change in state from a to b can be described by the change in only one variable. So, p_{01} may be thought of as the probability of having 0 cells in one class (say the infectious class) at time t and 1 cell in the same (infectious) class at time $t + \Delta t$. When there is only one independent variable to change between times, this approach is relatively straightforward. However, in our case, we have three independent variables that define our disease state: \mathcal{T} , \mathcal{E} , and \mathcal{I} .

In response to this, we first grouped the exposed and infectious classes together such that the state of the exposed/infectious class can be represented as an ordered pair of the form $(\mathcal{E}, \mathcal{I})$. Then we can form a transition matrix that describes the probability of transitioning in and out of this exposed/infectious class. There are $N + 1$ different matrices of this type that can be formed, where for each matrix the number of target cells, $\mathcal{T}(t) \in \{0, 1, 2, \dots, N\}$, is fixed. The form of these matrices is described in more depth below. Each of these matrices should be a part of our transition matrix, so our final transition matrix will appear as block matrix that is composed of these smaller matrices on the diagonal. This allows for the transition matrix to account for changes in the number of exposed/infectious cells, but we also need to account for changes in the remaining independent variable, \mathcal{T} .

The diagonal of our transition matrix is composed of the blocks described above, so we use the off-diagonal blocks to include diagonal matrices, denoted as $D_{\mathcal{T}(t), \mathcal{T}(t+\Delta t)}$, that account for the probability of transitioning between the $\mathcal{T}(t)$ and $\mathcal{T}(t + \Delta t)$

number of target cells. Like so:

$$\mathcal{M} = \begin{bmatrix} \left[\mathcal{T}(t) = 0 \right] & D_{0,1} & & & 0 \\ D_{1,0} & \left[\mathcal{T}(t) = 1 \right] & D_{1,2} & & \\ & D_{2,1} & & \ddots & \\ & & \ddots & \ddots & \\ 0 & & & D_{N,N-1} & \left[\mathcal{T}(t) = N \right] \end{bmatrix}.$$

In order to compute the probabilities contained in the transition matrix, we need to determine how a cell can move between our independent classes. Given that we end up with $(\mathcal{T}, (\mathcal{E}, \mathcal{I})) = (t + k, (e + j, i + l))$ at time $t + \Delta t$, we want to find all the states we could have been in at time t . We assume Δt is very small so that $\mathcal{T}(t)$, $\mathcal{E}(t)$, and $\mathcal{I}(t)$ can change by at most 1 in time Δt ; thus $k, j, l \in \{1, -1, 0\}$ (see the table below, table 3, for the events and how the event may lead to state $(t, (e, i))$).

Transition Events of Independent Variables

Event Description	State at t	State at $t + \Delta t$	(k, j, l)
Target cell becomes exposed	$(t + 1, (e - 1, i))$	$(t, (e, i))$	$(-1, 1, 0)$
Exposed cell becomes infectious	$(t, (e + 1, i - 1))$	$(t, (e, i))$	$(0, -1, 1)$
Infectious cell dies	$(t, (e, i + 1))$	$(t, (e, i))$	$(0, 0, -1)$
Cellular restoration	$(t - 1, (e, i))$	$(t, (e, i))$	$(1, 0, 0)$
No change	$(t, (e, i))$	$(t, (e, i))$	$(0, 0, 0)$

Table 3: Table describing the movements of each transition event to attain the $(t, (e, i))$ state.

The probabilities of the events described in the above table, table 3, are already known, and can be found in the first table. Using our knowledge of states at time t that could result in the state $(t, (e, i))$ at time $t + \Delta t$, and the transition probability between these states, we are able to find $P_{ab}(t + \Delta t)$, which can be thought of as the sum of the probabilities of transitioning into the state $b = (t, (e, i))$. The probability of remaining in state b during the time Δt has the probability: 1-(probability of

leaving state $(t, (e, i))$). Thus, we have the following lemma:

Lemma 1 For $t + e + i + d = N$, the probability of leaving state a and entering state b while $\mathcal{T}(t)$ remains fixed in time Δt is given by

$$(42) \quad P_{ab} = \sum_{\substack{e,i,j,l \geq 0 \\ e+i=a \\ e+j+i+l=b}} P_{(e,i),(e+j,i+l)}$$

where

$$(43) \quad P_{(e,i),(e+j,i+l)} = \begin{cases} \frac{e}{\tau_E} \Delta t & (j, l) = (-1, 1) \\ \frac{i}{\tau_I} \Delta t & (j, l) = (0, -1) \\ -\frac{e}{\tau_E} \Delta t - \frac{i}{\tau_I} \Delta t & (j, l) = (0, 0) \\ 0 & \text{otherwise.} \end{cases}$$

You may have observed that the transition probability associated with no change (i.e., when $(j, l) = (0, 0)$) should be $1 - \beta t \mathcal{V} \Delta t - r_D(N - t - e - i) \Delta t - \frac{e}{\tau_E} \Delta t - \frac{i}{\tau_I} \Delta t$ instead of $-\frac{e}{\tau_E} \Delta t - \frac{i}{\tau_I} \Delta t$; however, in some cases we may have several transitions in which $(j, l) = (0, 0)$. In these cases, we only want the $1 - \beta t \mathcal{V} \Delta t - r_D(N - t - e - i) \Delta t$ to appear in the sum once, where as $-\frac{e}{\tau_E} \Delta t - \frac{i}{\tau_I} \Delta t$ should appear as many times as the no change transition occurs. It is important to note that because of this discrepancy the ‘probabilities’ described above will be different from the actual probability when $a = b$. In this circumstance, the actual probability is

$$1 - \beta t \mathcal{V} \Delta t - r_D(N - t - e - i) \Delta t + P_{aa}, \quad \text{where } a \text{ is the state } (e, i).$$

We use the probabilities from Lemma 1 to determine the values in a matrix which we will call $M_{\mathcal{M}}$. To account for the extra added terms, we will form another matrix with the missing values, called M_R such that our transition matrix can be written as $\mathcal{M} = M_R + M_{\mathcal{M}}$.

We will denote our entire transition matrix as \mathcal{M} , where \mathcal{M} is the sum of two matrices, M_R and $M_{\mathcal{M}}$. We let M_R contain the off-diagonal blocks of \mathcal{M} and the remaining probability terms that are not generated in Lemma 1, these probabilities are all related to a change in the number of target cells. Each block describing the change in the number of target cells can be written in the form of a diagonal matrix denoted as $D_{\mathcal{T}(t), \mathcal{T}(t+\Delta t)}$.

In general, we have that

$$D_{\mathcal{T}(t), \mathcal{T}(t+\Delta t)} = \begin{bmatrix} \beta t \mathcal{V} \Delta t + r_D(N-t) & 0 & \dots & 0 \\ 0 & \beta t \mathcal{V} \Delta t + r_D(N-t-1) & \dots & 0 \\ \vdots & \vdots & \ddots & \vdots \\ 0 & 0 & \dots & \beta t \mathcal{V} \Delta t + r_D(0) \end{bmatrix}$$

where $t = \mathcal{T}(t)$. However, it is helpful to break $D_{\mathcal{T}(t), \mathcal{T}(t+\Delta t)}$ into the sum of two matrices, described below. Let $D_{\mathcal{T}(t), \mathcal{T}(t+\Delta t)} = B_{N-\mathcal{T}(t)+1} + C_{N-\mathcal{T}(t)+1}$, where the subscripts indicate the size of the matrix. $I_{N-\mathcal{T}(t)+1}$ is the $(N - \mathcal{T}(t) + 1) \times (N - \mathcal{T}(t) + 1)$ identity matrix, and

$$B_{N-\mathcal{T}(t)+1} = \begin{bmatrix} \beta t \mathcal{V} \Delta t & 0 & 0 & \dots & 0 \\ 0 & \beta t \mathcal{V} \Delta t & 0 & \dots & 0 \\ 0 & 0 & \beta t \mathcal{V} \Delta t & \dots & 0 \\ \vdots & \vdots & \vdots & \ddots & \vdots \\ 0 & 0 & 0 & \dots & \beta t \mathcal{V} \Delta t \end{bmatrix},$$

$$C_{N-\mathcal{T}(t)+1} = \begin{bmatrix} r_D(N-t)\Delta t & 0 & 0 & \dots & 0 \\ 0 & r_D(N-t-1)\Delta t & 0 & \dots & 0 \\ 0 & 0 & r_D(N-t-2)\Delta t & \dots & 0 \\ \vdots & \vdots & \vdots & \ddots & \vdots \\ 0 & 0 & 0 & \dots & r_D(0)\Delta t \end{bmatrix}.$$

Thus, $B_{N-\mathcal{T}(t)+1}$ is a matrix containing the probabilities of one of the $\mathcal{T}(t)$ targets cell becoming exposed, and $C_{N-\mathcal{T}(t)+1}$ is a matrix containing the probabilities of a dead cell becoming a target cell via cellular restoration. Writing D as the sum of these two matrices is useful for writing M_R , because we are now able to define M_R in the following manner:

$$M_R = \begin{bmatrix} I_{N+1} - B_{N+1} - C_{N+1} & C_{N+1} & 0 & 0 & \dots & 0 \\ B_N & I_N - B_N - C_N & C_N & 0 & \dots & 0 \\ 0 & B_{N-1} & I_{N-1} - B_{N-1} - C_{N-1} & C_{N-1} & \dots & 0 \\ \vdots & \vdots & \vdots & \ddots & \ddots & \vdots \\ \vdots & \vdots & \vdots & \ddots & \ddots & C_2 \\ 0 & 0 & 0 & \dots & B_1 & I_1 - B_1 - C_1 \end{bmatrix}.$$

$M_{\mathcal{M}}$ contains the small transition matrices along the diagonal of \mathcal{M} with the transition probabilities from Lemma 1. The smaller transition matrices for fixed \mathcal{T} values which exist on the diagonals of \mathcal{M} will be denoted as \mathcal{M}_t ; where the subscript is the fixed number of target cells. Using the probabilities from Lemma 1, we can generate a general description of a \mathcal{M}_t matrix.

$$\begin{aligned} \mathcal{M}_t &= \begin{bmatrix} 0 & 0 & 0 & 0 & \dots & 0 & 0 \\ 0 & \frac{2}{\tau_I}\Delta t & -\frac{2}{\tau_I}\Delta t & 0 & \dots & 0 & 0 \\ 0 & 0 & \frac{3}{\tau_I}\Delta t & -\frac{3}{\tau_I}\Delta t & \dots & 0 & 0 \\ \vdots & \vdots & \vdots & \ddots & \ddots & & \vdots \\ \vdots & \vdots & \vdots & & \ddots & \ddots & \vdots \\ 0 & 0 & 0 & 0 & \dots & -\frac{N-t}{\tau_I}\Delta t & -\frac{N-t}{\tau_I}\Delta t \end{bmatrix} \\ &= \begin{bmatrix} P_{00} & P_{01} & \dots & P_{0(N-t)} \\ P_{10} & P_{11} & \dots & P_{1(N-t)} \\ \vdots & \vdots & \ddots & \vdots \\ P_{(N-t)0} & P_{(N-t)1} & \dots & P_{(N-t)(N-t)} \end{bmatrix} \end{aligned}$$

Using the notation described above, we are able to write our finished transition matrix, \mathcal{M} as the sum of the matrices M_R and $M_{\mathcal{M}}$, where M_R is as described above, and

$$M_{\mathcal{M}} = \begin{bmatrix} \mathcal{M}_0 & 0 & 0 & \dots & 0 \\ 0 & \mathcal{M}_1 & 0 & \dots & 0 \\ 0 & 0 & \mathcal{M}_2 & \dots & 0 \\ \vdots & \vdots & \vdots & \ddots & \vdots \\ 0 & 0 & 0 & \dots & \mathcal{M}_N \end{bmatrix}.$$

Notice that all rows of any \mathcal{M}_t matrix sum to 0. Since the remaining entries in $M_{\mathcal{M}}$ are all 0, we can see that any row in $M_{\mathcal{M}}$ sums to 0. In the matrix M_R , B_{N+1} and C_1 are both Zero-matrices, so adding matrices row-wise sums to the identity matrix, which has 1's along the diagonal and 0 everywhere else. Thus, every row in M_R sums to 1. Since every row in M_R sums to 1 and every row in $M_{\mathcal{M}}$ sums to 0, we can see that every row in \mathcal{M} sums to $1+0 = 1$. So, we have confirmed that \mathcal{M} meets the condition to be a transition matrix.

To use \mathcal{M} as our transition matrix, there is still one problem we need to address. The way \mathcal{M} is described above still contains a random variable \mathcal{V} . Since we do not want any random variables in our matrix, this is something that needs to be changed. \mathcal{V} represents the amount of virus that is present, and because the virus is produced by infectious cells, we would expect the amount of virus to be a function of both the number of infectious cells, and the production rate at which infectious cells produce new virions. Thus, we let $\mathcal{V} = \mathcal{V}(i) = p \cdot i$, where $i = \mathcal{I}(t)$. When we go to replace \mathcal{V} with $p \cdot i$, we run into a new problem; what is the value of $\mathcal{I}(t)$? Recall that the exposed and infectious classes were grouped together, so at any point in the transition matrix, if we have a exposed/infectious cells at time t and b , exposed/infectious cells at time $t + \Delta t$, how many infectious cells are there at time t ? The term \mathcal{V} only appears on the main diagonal of \mathcal{M} and in the B_{N-t} off-diagonal matrices. Recall also that each row of the transition matrix must sum to 1, so the value of \mathcal{V} must be the same in both places it appears in one row; this allows us to focus on the value of $\mathcal{I}(t)$ on the main diagonal.

Let $y = e+i$, then y is the total number of exposed/infectious cells at time t , which functions as the index of the rows of \mathcal{M}_t . Consider the diagonal entry of an arbitrary y th row of \mathcal{M}_t . The value of this entry represents the probability of transitioning from y exposed/infectious cells to y exposed/infectious cells in time Δt , when there are $\mathcal{T}(t) = t$ target cells. We make a table of all transitions of y exposed/infectious cells to y exposed/infectious cells that have a non-zero probability.

We wish to find the expected value of i at time t when we transition from y to y exposed/infectious cells. This is given by the below lemma.

Lemma 2 The expected number of infectious cells at time t when transitioning from y exposed/infectious cells to y exposed/infectious cells is denoted $\mathbb{E}(i)$, and is given by

$$\mathbb{E}(i) = \frac{y^2}{2y + 1}.$$

Implications of Lemma 2: Any time we know the combined number of exposed/infectious cells, y , we can calculate the expected number of infectious cells. We may also use this to replace the random variable \mathcal{V} with the virus production rate per infectious cell times the expected number of infectious cells, $V(y) = p \cdot \frac{y^2}{2y+1}$. Thus, we are able

Transition Events with a Fixed Number of Exposed/Infectious Cells, y

(e, i) at time t	$(e + j, i + k)$ at time $t + \Delta t$	Event Description
$(y, 0)$	$(y, 0)$ $(y - 1, 1)$	No change Exposed cell becomes infectious
$(y - 1, 1)$	$(y - 1, 1)$ $(y - 2, 2)$	No change Exposed cell becomes infectious
\vdots	\vdots	\vdots
$(1, y - 1)$	$(1, y - 1)$ $(0, y)$	No change Exposed cell becomes infectious
$(0, y)$	$(0, y)$	No change

Table 4: Possible transition events starting with $e + i = y$ exposed/infectious cells.

to eliminate all random variables from our matrix. Lemma 2 also provides us with the ability to approximate the number of infectious cells at any time point in our stochastic simulations.

Proof/reasoning of Lemma 2: From table 4, we see that there are $y + 1$ different states at time t , corresponding to $i = 0, 1, \dots, y$. The first y of these states have 2 possible outcomes, no change or an exposed cell becoming infectious. The only exception is for the case when $i = y$ at time t , which only has one outcome because there are no exposed cells to become infectious. Thus, there are $2y + 1$ possible events.

$$\begin{aligned}
 \mathbb{E}(i) &= \frac{2}{2y+1}(0) + \frac{2}{2y+1}(1) + \dots + \frac{2}{2y+1}(y-1) + \frac{1}{2y+1}y \\
 &= \frac{2}{2y+1}(0+1+\dots+y-1) + \frac{y}{2y+1} \\
 (44) \quad &= \frac{2}{2y+1} \cdot \frac{(y-1)y}{2} + \frac{y}{2y+1} \\
 &= \frac{y^2}{2y+1}.
 \end{aligned}$$

Recall that given a transition probability matrix, \mathcal{M} , and a vector describing the state of the disease at time t_0 , which we will call $X(t_0)$, one may determine the vector

describing the likely state of the disease at time $t_0 + n\Delta t$, $X(t_0 + n\Delta t)$ by

$$X(t_0 + n\Delta t) = \mathcal{M}^n X(t_0).$$

To carry out these sorts of computations, we need to know the form of the vector $X(t)$ that describes the state of the disease at time t . Since $X(t)$ will be multiplied by \mathcal{M} , and \mathcal{M} is a $\frac{(N+1)(N+2)}{2} \times \frac{(N+1)(N+2)}{2}$ matrix, we know that $X(t)$ must be a vector of length $\frac{(N+1)(N+2)}{2}$. This makes sense because there are $\frac{(N+1)(N+2)}{2}$ possible states of the form (t, y, d) , where $t = \mathcal{T}(t)$, $y = e + i$, and $d = \mathcal{D}(t)$; and $X(t)$ is a vector containing the probabilities of being in each of these states.

Recall also that \mathcal{M} is a block-diagonal matrix, where each sub-matrix on the diagonal is similar to a transition probability matrix where the number of target cells is fixed. If the fixed number of target cells is $\mathcal{T}(t)$, then the size of sub-matrix corresponding to this number of target cells is $(N - \mathcal{T}(t)) \times (N - \mathcal{T}(t))$. There should be a corresponding section of the vector $X(t)$ that has a length of $N - \mathcal{T}(t)$, as demonstrated in figure 2.

Form of Transition Matrix and Disease-State Vector

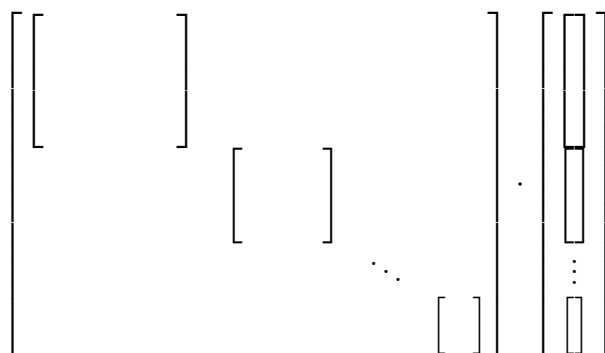


FIGURE 2. Basic form of Transition Matrix and Disease-State Vector. The boxed areas indicate regions corresponding to a fixed number of target cells.

The initial state vector, $X(t_0)$ should be able to specify exactly what state of the disease we are starting with. Since we want to begin with certainty as to which state we are in at t_0 , we know that $X(t_0)$ should be a vector containing one 1 at the entry that represents part of our vector that defines the initial disease state, and 0's everywhere else. Thus, if we start with $N - 3$ target cells, then the vector $X(t_0)$ should contain only 0's except for the third to last section of the vector. This section of the vector should be the same size as the third to last block of the matrix \mathcal{M} . This matrix has a size of $(N - (N - 3) + 1) \times (N - (N - 3) + 1)$ or 4×4 , thus the corresponding part of $X(t_0)$ has four entries.

If there are $N - 3$ target cells, then there are 3 cells remaining that fall into some other class; namely the exposed/infectious class, or the dead class. There could be 0, 1, 2, or 3 exposed/infectious cells. Since $y + d = 3$ in this case, we have four possible states of the form (t, y, d) : $(N - 3, 0, 3)$, $(N - 3, 1, 2)$, $(N - 3, 2, 1)$, or $(N - 3, 3, 0)$. In fact, in general, if there are $N - n$ target cells, then there can be 0, 1, 2, ..., n exposed/infectious cells, forming $n + 1$ possible states that are represented by an $n + 1$ length section of $X(t_0)$.

Since the section of $X(t_0)$ that corresponds to $\mathcal{T}(t)$ has the same number of rows as $\mathcal{M}_{\mathcal{T}(t)}$, we would expect the rows of that part of $X(t_0)$ and the rows of $\mathcal{M}_{\mathcal{T}(t)}$ to represent the same thing. Say, we wanted to start with 1 exposed/infectious cell. Since there are $N - 3$ target cells, this means that there are 2 dead cells. The rows of $\mathcal{M}_{\mathcal{T}(t)}$ represent the number of exposed/infectious cells before the time Δt has passed. So, having 1 exposed/infectious cell would put us in the second row, because the first row refers to having 0 exposed/infectious cells. Thus, the corresponding

part of $X(t_0)$ is $\begin{bmatrix} 0 \\ 1 \\ 0 \\ 0 \end{bmatrix}$.

Thus, if we wanted our initial disease state to be $N-3$ target cells, 1 exposed/infectious cell, and 2 dead cells, then we have

$$X(t_0) = \begin{bmatrix} 0 \\ 0 \\ \vdots \\ 0 \\ 1 \\ 0 \\ 0 \\ \vdots \\ 0 \end{bmatrix} .$$

4. NUMERICAL SIMULATIONS

Numerical Simulation of the Deterministic Model



FIGURE 3. An example of the Deterministic Solutions' trajectories reaching an endemic equilibrium when $\mathcal{R}_0 > 1$.

4.1. Stochastic Simulations. Using our transition matrix and a vector describing an initial disease state, we can simulate the expected trajectory of the disease by repeatedly multiplying the initial state vector by the transition matrix. Every time we multiply by the transition matrix, we move forward by Δt in time. As stated previously Δt must be chosen to be small enough so that multiply events do not occur simultaneously. When Δt is chosen to be too large, the simulation breaks down and produces impossible results (such as probabilities as large as 10^{136}), so this problem is quite easy to spot. When Δt is chosen to be too small, then the probability of an event occurring during the time Δt is too small and the simulation indicates that there is no change from the initial state, even after a large number of iterations. Thus, there is an ideal range for the value of Δt . Due to our complexity, the ideal size of Δt depends on the number of cells that are being simulated, so a relationship between N and Δt needs to be established. In order to determine the appropriate form of this relationship, we first collected data on the bounds of Δt for each N to produce the following graph.

If we let $\Delta t = 10^{-i}$ for some $i \in \mathbb{N}$, then the ideal region for i appears to follow an approximately linear path in relation to N . We let Δt be on the larger end of the ideal range for two reasons: problems due to Δt being too large are easy to spot and a larger Δt saves computation. This linear path is approximated from the points (100, 9.5) and (30, 8) from figure 4, and we obtain $-(\frac{3}{140}N + \frac{103}{14})$. So, we let $\Delta t = 10^{-\lfloor \frac{3}{140}N + \frac{103}{14} \rfloor}$ to simulate our stochastic model.

There are several patterns that appear in the stochastic simulations that occur at different time scales. We will begin with the smallest time scale and work our way to a larger scale.

Simulation using 80000 or less iterations:

We begin by looking at what occurs when we simulate $\mathcal{M}^n \cdot X(0)$ for $0 \leq n \leq 80000$. This produces a wave-like pattern, which can be seen in figure 5.

We observe that as the probability of one state begins to decline, the probability of one other state rises. This propagates the most likely state down to an eventual end state, at which point, the probability of this last state appears to approach 1.

Ideal Δt for N Cells

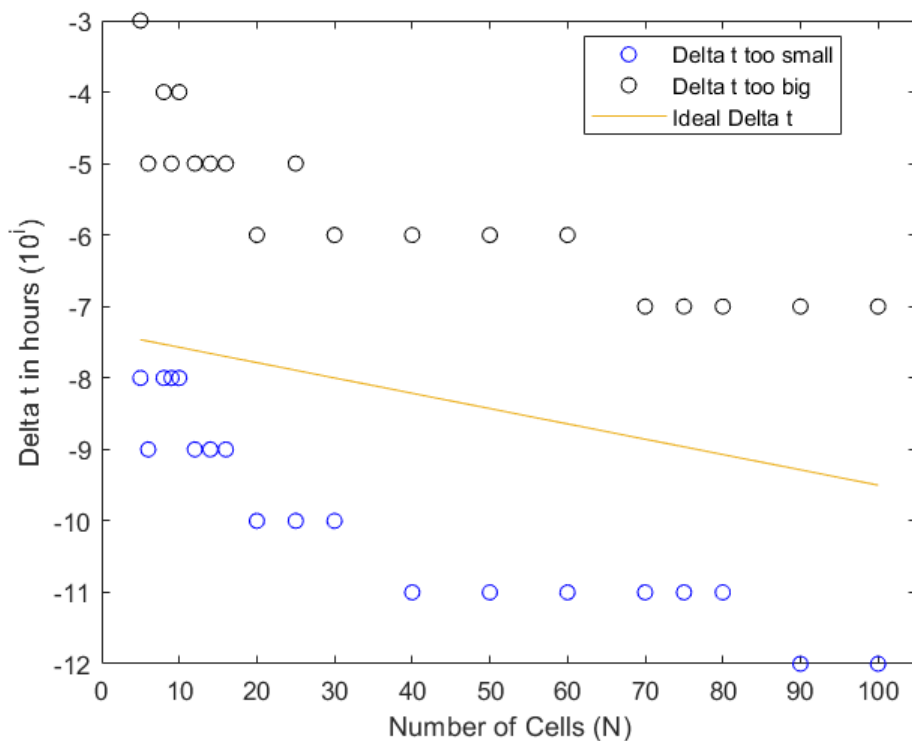


FIGURE 4. Scatterplot of the boundaries for Δt for $0 \leq N \leq 100$ with function for the ideal Δt .

Upon close examinations of the most probable states at any given time, we see that it is easy to predict the course of the simulation, given the initial vector. We give an example of a simulation with a relatively small number of cells. In figure 5, we see that there are five states with non-zero probabilities. The initial state (the spike with probability 1 seen at iteration 0) can be represented by the ordered triplet $(4, 21, 0)$, which is of the form (t, y, d) . The next state that emerges after approximately 1000 iterations is $(3, 22, 0)$. The next state that peaks in probability is $(2, 23, 0)$, then $(1, 24, 0)$, and finally, the last state that appears is $(0, 25, 0)$. So, we have the following sequence between states:

$$(4, 21, 0) \rightarrow (3, 22, 0) \rightarrow (2, 23, 0) \rightarrow (1, 24, 0) \rightarrow (0, 25, 0).$$

State Probabilities of 25 cells over Time

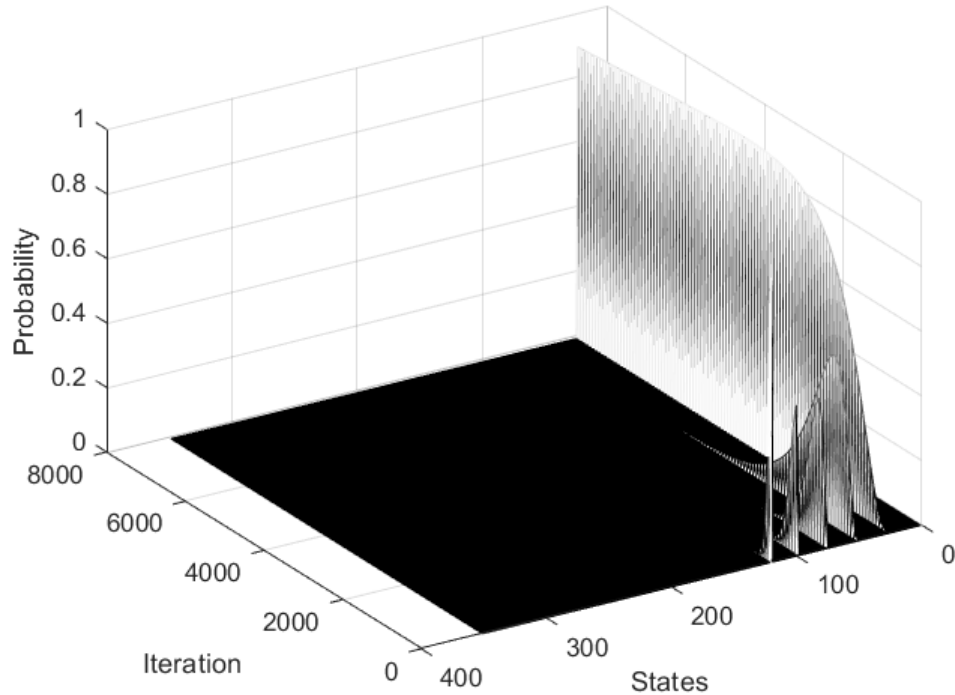


FIGURE 5. Probability of each state for 25 cells over 8000 iterations (approximately 2.88 seconds) starting at the disease state $(4,21,0)$.

Notice that the initial number of dead cells is always the most likely number of dead cells, meaning that if the initial disease state is (t_0, y_0, d_0) , then states with non-zero probabilities will be of the form (t_n, y_n, d_0) for $0 \leq n \leq 80,000$. One can also see that the target cells tend to become exposed/infectious cells while the number of dead cells remain constant. Thus, on this time scale, we see that initial states of the form (t_0, y_0, d_0) go to $(0, y_0 + t_0, d_0)$ within 0 to 80000 iterations. This pattern can be viewed with a larger number of cells and appears regardless of initial disease state.

Without looking further, we might be led to believe that given an initial disease state of (t_0, y_0, d_0) , that the disease approaches the state $(0, y_0 + t_0, d_0)$ as $t \rightarrow \infty$;

State Probabilities of 100 cells over Time

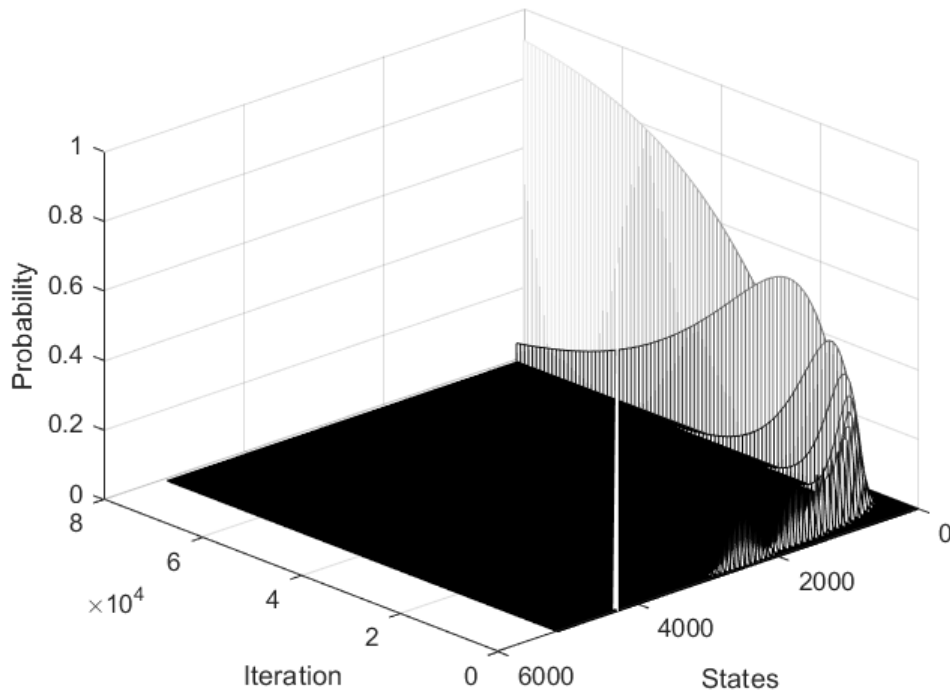


FIGURE 6. Probability of each state for 100 cells over 80000 iterations (approximately 0.43 seconds) starting at the disease state (60,5,35) and approaching the state (0,65,35).

however, this does not appear to be the case.

Simulations using 80000 to 600000 iterations:

If we look at time values beyond 80000 iterations, we see that the probability of the $(0, y_0 + t_0, d_0)$ state decreases, as the probability of $(0, y_0 + t_0 - 1, d_0 + 1)$ increases. This new transition in probabilities occurs much slower, and the next state does not fully surpass the $(0, y_0 + t_0, d_0)$ state until approximately $t_0 + 550000\Delta t$ for the simulations displayed in figure 7.

State Probabilities of 25 cells over Time

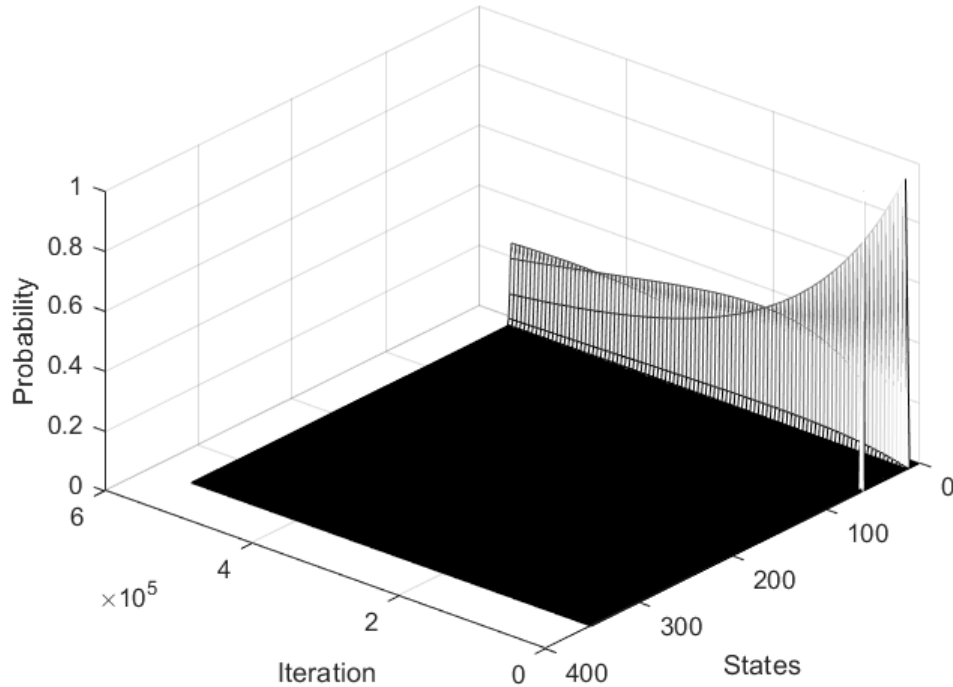


FIGURE 7. Probability of each state for 25 cells over 550000 iterations (approximately 3.3 minutes) starting at the disease state (2,8,15).

In the simulation in figure 7, we use $N = 25$ cells. The first several spikes demonstrate the pattern described above. The initial state (2,8,15), transitions to (0,10,15), which completes the sequence of states described above. The end of this sequence is recognizable, because the state that it leads to, the state (0,10,15) with all target cells having become infected occurs with very high probability. This high probability is sustained for some time, but as one can see in the above figure, that a new state (0,9,16) eventually surpasses this peak disease state in probability, which is in turn surpassed by the state (0,8,17).

Subsequently, if we focus on a larger time scale, we see a new wave of high-probability states begin, forming a progression from (0,8,17) to (0,7,18), (0,6,19), (0,5,20), (0,4,21), (0,3,22), (0,2,23), (0,1,24) and eventually (0,0,25). Once there

are 0 target and 0 exposed/infectious cells, the probability of state $(0, 0, d_0 + t_0 + y_0)$ appears to approach 1. Only the start of this progression can be seen in figure 7, however, this full pattern can be seen in figure 8. It becomes very computationally expensive to run simulations involving more than 8 million iterations, especially for large N , thus it is unclear if this the state $(0, 0, d_0 + t_0 + y_0)$ persists, or if new state with higher probabilities eventually arise. This is a source for future research.

State Probabilities of 5 cells over Long-Term

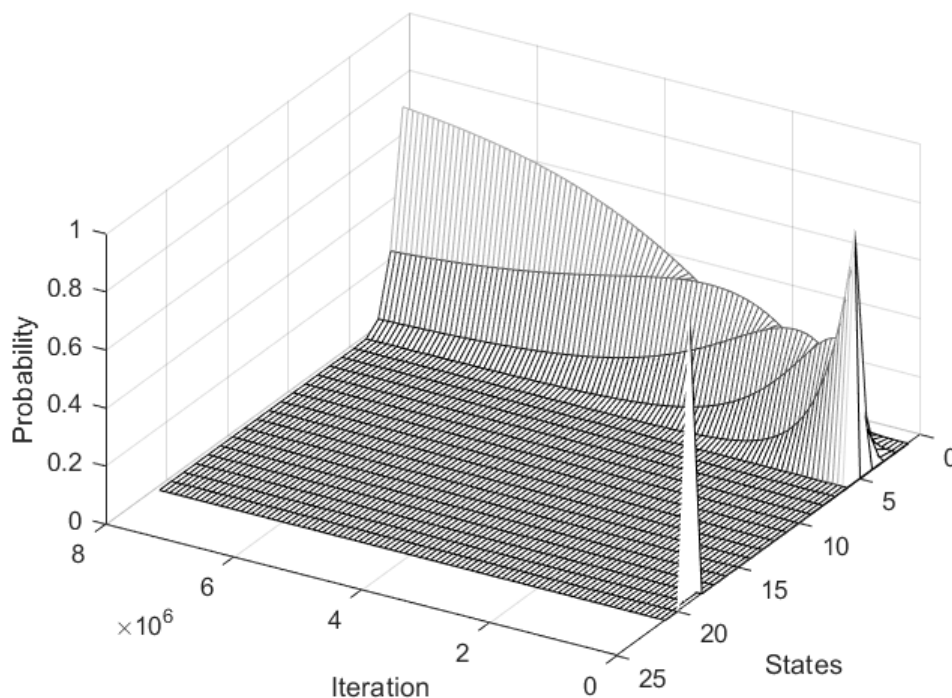


FIGURE 8. Probability of each state for 5 cells over 8000000 iterations (approximately 48 minutes) starting at the disease state $(4,0,1)$.

5. SENSITIVITY ANALYSIS

Sensitivity analysis allows us to determine which parameters are most influential to the model output. We use this information to examine biological implications such as model corroboration, research prioritization, model simplification, identification

of critical areas, and baseline parameter estimates [44, 34]. We will start the Latin Hypercube Sampling (LHS) method which will give us the necessary information to rank our parameters' degree of importance through the Partial Rank Correlation Coefficient (PRCC) method.

LHS is a stratified sampling without replacement technique, first introduced by McKay et. al. in 1979, that allows us to sample the entire parameter space more efficiently than similar Monte Carlo methods. LHS splits each of the k parameter distributions into N equally probable parts where N is at least greater than $k + 1$, although it is often much greater for the sake of accuracy. These distributions are used to create the LHS input matrix. This matrix has N rows, one for each simulation, and k columns, one for each parameter. The k^{th} entry of each row randomly selects an interval from the given parameter's probability distribution without replacement. This process is repeated to create N unique combinations of the parameters that spans the entire parameter space.

From this, a $N \times 1$ output matrix is generated where each entry is the output value from the corresponding simulation. Both the input and output matrices are then rank transformed according to the magnitude of the values along a column. The rank transformed matrices replace the raw data with values from one to N . We complete this transformation in order to compute the PRCC values which are explained below [33].

Before choosing PRCC, it is important to check for monotonicity between parameters and outputs. If we lack this, PRCC values are not accurate. If monotonicity does not hold, it is sometimes possible to truncate the LHS parameter ranges into monotonic regions [21].

PRCC uses the rank transformed data, not the raw data, to provide a measure of the linear association between a specific parameter and the output after the linear effects from the remaining inputs are removed. PRCC values range from -1 to 1, where a positive sign indicates a direct relationship between the parameter and the output value while a negative sign indicates an inverse relationship between the two. The magnitude of the PRCC value represents the importance of the parameter to the model output. The further the value is from zero, the more influential it is [33].

The *E Cases* output measure is defined by $\beta TV - \frac{E}{\tau_E}$. When we look at these graphs shown in figure 9, we are considering the relationship between the given

Monotonicity Plots

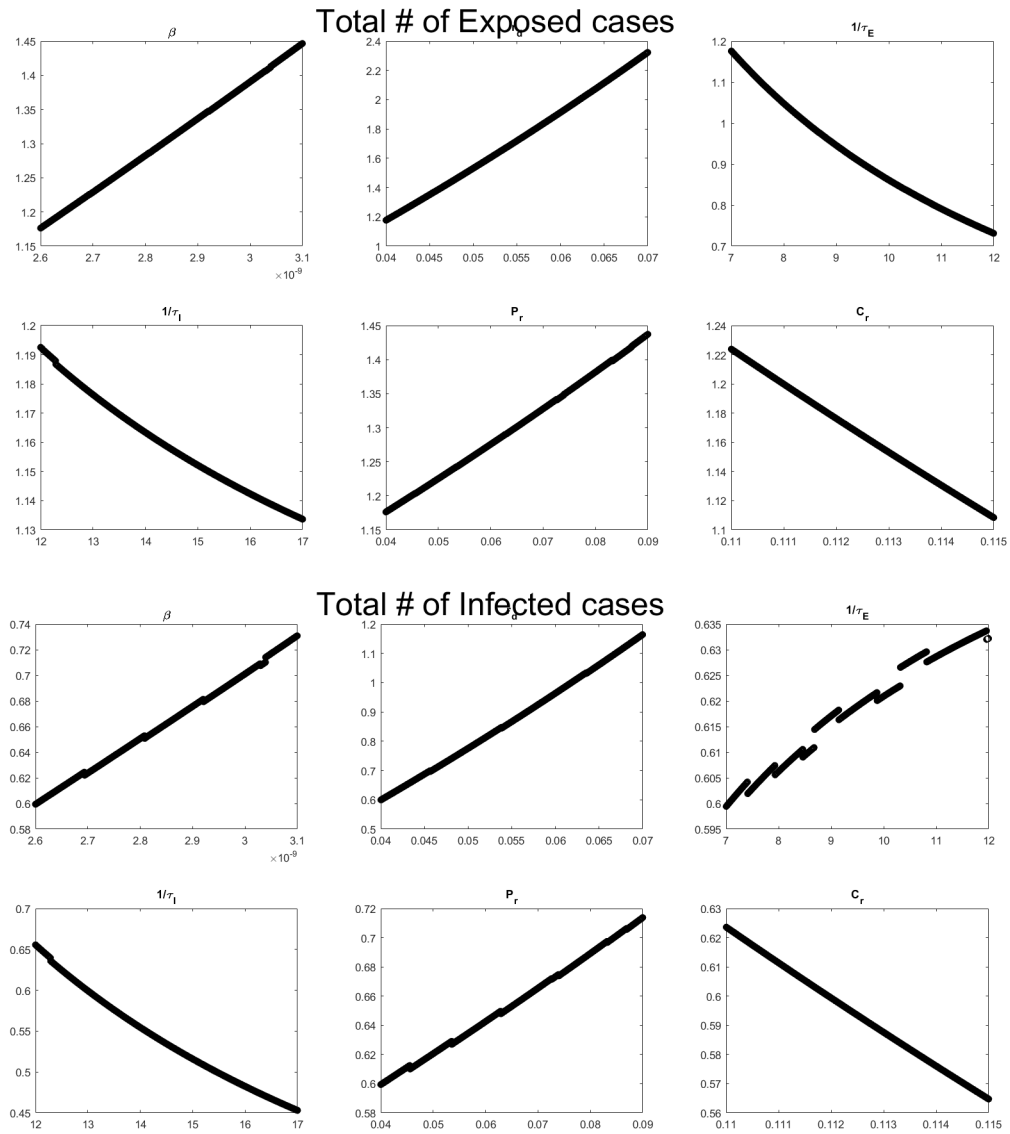


FIGURE 9. The title of the given section of graphs is the output measure for the given case and is along every y-axis. The parameter above every individual graph lies on the x axis.

Monotonicity Plots Cont.

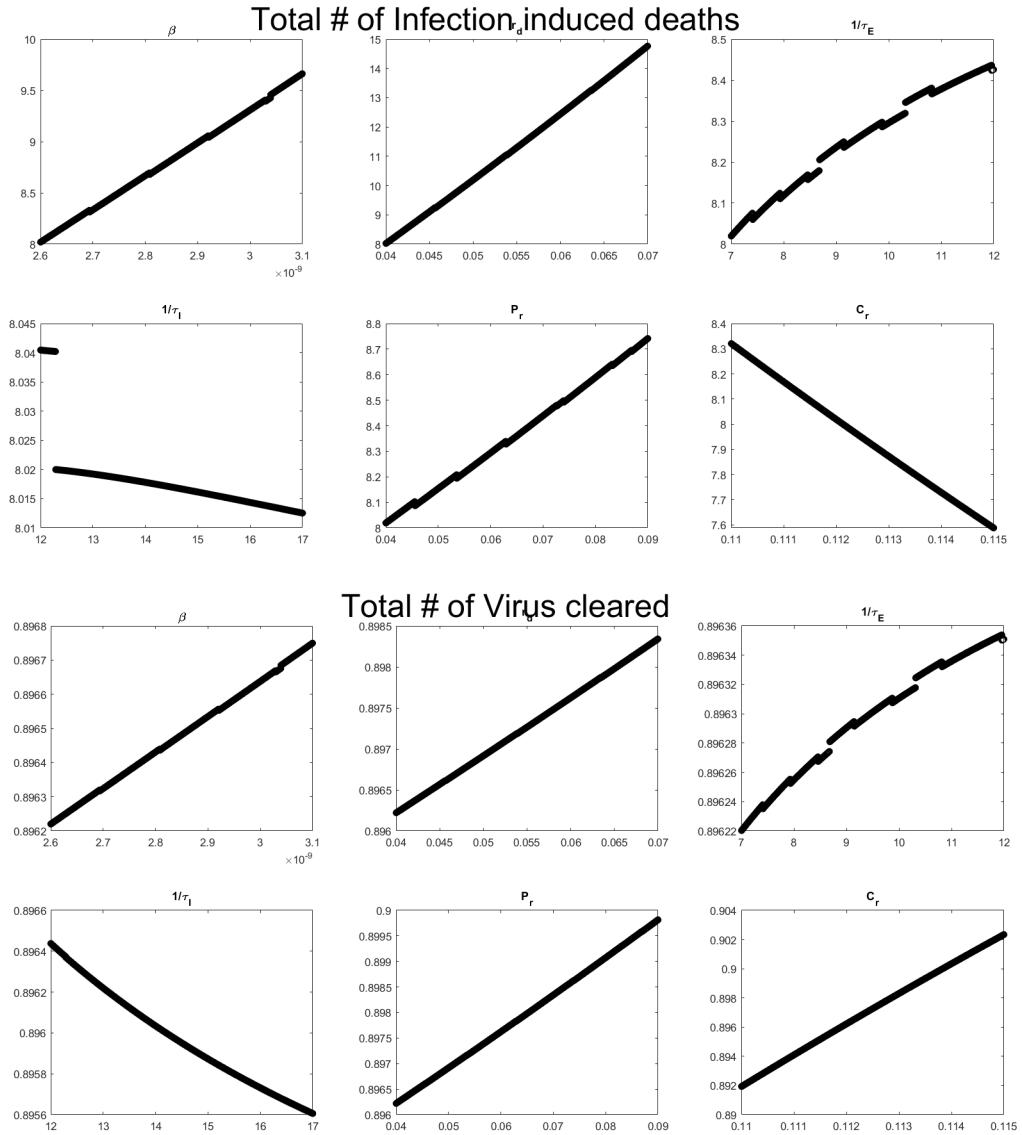


FIGURE 10. The set up is the same at the above graphs.

parameter and the difference between cells entering the E compartment, βTV , and

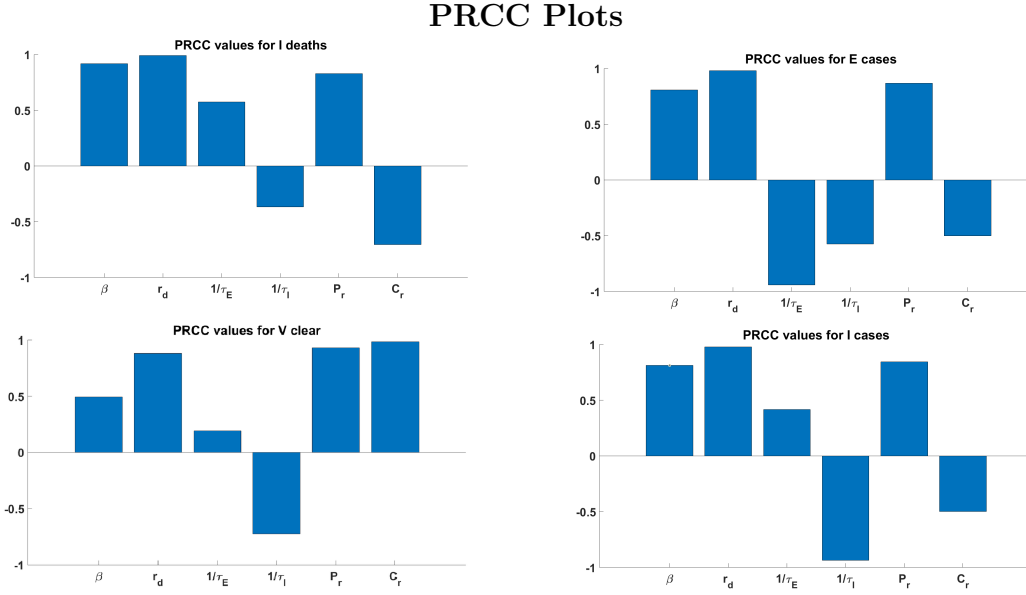


FIGURE 11. On the y axis we have the PRCC values and along the x axis each bar corresponds with the given parameter

the cells exiting the the E compartment, $\frac{E}{\tau_E}$. The parameter lies on the x axis in the shown graphs. It is important to note that all these plots are monotonic, so we can go on to consider the PRCC values as accurate. From figure 11, the parameters' degree of influence on the *E Cases* output measure ranked from least to greatest are: $c < \frac{1}{\tau_I} < \beta < p < \frac{1}{\tau_E} < r_D$. $\frac{1}{\tau_E}, \frac{1}{\tau_I}$ and c have an inverse relationship with the output while β, r_D and p have a direct relationship on the data. It is interesting to note that the parameters with positive PRCC values all fall into the numerator of \mathcal{R}_0 while the parameters with negative PRCC values fall into the denominator.

The number of infectious cases is measured by $\frac{E}{\tau_E} - \frac{I}{\tau_I}$, this is referred to as *I Cases* in the associated plots shown in 9. From figure 11, the parameters that impact the number of infectious cases listed from least to most impact are: $\frac{1}{\tau_E} < c < \beta < p < \frac{1}{\tau_I} < r_D$, where the parameters r_D, p , and β are directly proportional to the number of infectious cases and the parameters $\frac{1}{\tau_I}$ and c are inversely proportional to the number of infectious cases. We notice that for the number of infectious cases, parameters that are directly proportional to *I cases* that also appear in \mathcal{R}_0 are the

parameters that appear in the numerator of \mathcal{R}_0 ; namely p and β . Similarly, the parameters that are inversely proportional to I cases that also appear in \mathcal{R}_0 are the parameters that appear in the denominator of \mathcal{R}_0 ; specifically $\frac{1}{\tau_I}$ and c .

The number of infection induced deaths is calculated using $\frac{I}{\tau_I}$ which is shown in figure 10. The parameters that impacts the number of infection induced deaths, written as I deaths, ranked from least to most impactful to get $\frac{1}{\tau_I} < \frac{1}{\tau_E} < c < p < \beta < r_D$, this is again from figure 11. Parameters that are directly proportional to the number of infection induced deaths are r_D , β , p , and $\frac{1}{\tau_E}$, while parameters that are inversely proportional to the number of infection induced deaths are c and $\frac{1}{\tau_I}$. The same relationship can be seen between the proportionality of parameters and \mathcal{R}_0 in E cases and I cases can be seen in I deaths.

The number of virions cleared is given by cV , shown in figure 10, is effected by the following parameters, ranking from least to the most impactful, as shown in figure 11: $\frac{1}{\tau_E} < \beta < \frac{1}{\tau_I} < r_D < p < c$. The parameters c , p , r_D , β , and $\frac{1}{\tau_E}$ are all directly proportional to the amount of virus cleared, whereas $\frac{1}{\tau_I}$ is inversely proportional to the number of virions cleared. Since c is directly proportional to this measure, we do not see the same pattern related to \mathcal{R}_0 as we did in the previous measures. This change follows our assumption, however, due to the amount of virus cleared not being directly related to the trajectory of the virus. When V clear is very high, it could either be due to the host being very efficient at clearing out the virus, or it could be because the host is sustaining the virus for a long time. Thus, the value of V clear is not clearly related to whether the state of the virus is approaching endemic or disease-free equilibrium.

Sensitivity analysis revealed that r_D , p , and β are directly proportional to all four measures of the disease. $\frac{1}{\tau_I}$ was found to be inversely proportional to all four measures of the disease, and clearance rate, c , was found to be inversely proportional to the number of exposed cases, the number of infectious cases, and the number of disease-induced deaths.

In the monotonicity plots, we can observe that the plot corresponding to $\frac{1}{\tau_E}$ is not strictly monotonic. Sensitivity analysis using PRCC requires monotonicity, thus this may be a source of error in our analysis.

The ranking of how much each parameter affects the number of exposed cases, infectious cases, cell deaths, and virions cleared is consistent regardless of the number of runs used. However, the magnitude of the PRCC values does change depending on the number of runs used. In some cases, this difference is extreme; such as when comparing the PRCC values of $\frac{1}{\tau_E}$ and β for the number of virions cleared using 100 runs to the PRCC values of $\frac{1}{\tau_E}$ and β for the number of virions cleared using 2000 runs. When using 100 runs, $\frac{1}{\tau_E}$ has a PRCC value of 0.033 and β has a PRCC value of 0.523, making for a 0.490 difference. When using 2000 runs, $\frac{1}{\tau_E}$ has a PRCC value of 0.192 and β has a PRCC value of 0.493, making a difference of 0.301. The degree to which the difference between the PRCC values of $\frac{1}{\tau_E}$ and β changes depending on the number of runs is concerning and may be the result of the non-monotonicity of $\frac{1}{\tau_E}$. Since the largest number of simulations used (in this case $N = 2000$) should be the most accurate, we will examine the results when that number of runs is used. For information regarding the 100, 500, and 1000 runs, see the appendix.

For 2000 simulations, the PRCC values of each parameter all have $p < 1.2 \cdot 10^{-9}$, so each parameter significantly effects the number of expose cases, infectious cases, deaths due to infection, and virions cleared.

6. DISCUSSION

The Basic Reproduction Number, \mathcal{R}_0 was calculated to be $\frac{\beta p N}{c \frac{1}{\tau_I}}$. The numerator of \mathcal{R}_0 , $\beta p N$, contains values related to the transmission and production of the virus, and the denominator, $c \frac{1}{\tau_I}$, contains values related to the death and clearance of the virus. Thus, when the production and transmission of the virus is greater than the death and clearance of the virus, we see a spread in infectious and a tendency to the locally asymptotically stable endemic equilibrium. On the other hand, when production and transmission is less than the death and clearance of the virus, the disease tends to the locally asymptotically stable disease-free equilibrium. The goal in influenza treatment then, would be to manipulate the conditions of the disease in order to produce a situation that approaches the disease-free equilibrium. Thus, it

is important to determine what parameters contribute the most to hallmarks of the disease.

Partial Rank Correlation Coefficients were used to determine how different parameters contributed to important measures of the disease including, the number of exposed cases, the number of infectious cases, the number of infection-induced deaths, and the number of virions cleared. Health professionals would ideally like to minimize the first three of these measures. Interestingly, it was found that cellular restoration had the strongest positive relationship with the number of exposed cases, the number of infectious cases, and the number of cell deaths due to infection. This finding may indicate that in some cases it would be helpful to slow down cellular restoration as it is positively associated with the measures we wish to minimize. No causation is established in this study, however, the detrimental role of cellular restoration on the trajectory of the spread of influenza has been documented in other cases [15]. In particular, chronic cases of influenza cannot occur without cellular restoration, so this parameter clearly plays a role in the perpetuation of the influenza infection.

It was also noted from the sensitivity analysis that parameters that were directly proportional to the number of exposed cases, the number of infectious cases, and the number of disease-induced deaths tend to appear in the numerator of \mathcal{R}_0 , whereas parameters that are indirectly proportional to these measures tend to appear in the denominator of \mathcal{R}_0 . This makes sense because each of these three measure impact the trajectory of the disease (whether it tends to endemic state or disease-free), which is precisely what \mathcal{R}_0 measures.

Results from the stochastic simulations indicate that influenza first spreads extremely rapidly, achieving a state in which all target cells are either exposed or infectious very quickly. Comparatively, it takes a much longer time for the exposed and/or infectious cells to die. To illustrate; for a population of 5 cells with initially 0 exposed/infectious cells it takes approximately 10-11 seconds for all the original target cells to become exposed/infectious, and it is not until at least 3 minutes have passed since the initial time that the first cells begin to die. These findings indicate that any treatment for influenza intended to curtail the spread of the virus within the host would need to be administered and be effective very soon after initial exposure to the influenza virus. These findings are supported by biological evidence that

early administration of antiviral treatment for patients with influenza is an important factor of recovery [56].

7. FUTURE DIRECTIONS

In the future, due to the dependence of initial time and spatial dependence of the infection, it is imperative to account for the spatial component of within-host virus kinetics by utilizing a system of Partial Differential Equations. It would also be helpful to develop a more efficient method for simulating the stochastic model in order to better understand the end behavior of this model.

It is also important to compare the models developed in this article with data collected regarding the spread of influenza within-host. Doing so would allow us to verify the accuracy of our model as well as refine our models using parameter estimation. Currently, we are using values for our parameters that previous studies have used in their models [6, 7, 54]; however, it may be more beneficial to use collected biological data to estimate our parameters through a process known as parameter estimation. For details about how we would approach parameter estimation, see the appendix.

It would be possible to utilize the results from the stochastic simulations to determine the time until peak infection (when the maximum number of exposed and infectious cells is achieved). This time appears to depend both on the number of cells present, N , as well as the initial state. In particular, it may be useful to examine how the initial number of infectious cells impacts the time until peak infection and if/how the relationship is mediated by N . The tools developed in this study are sufficient to investigate this question, but due to the computationally expensive nature of the simulations, this question remains unanswered.

8. APPENDIX

8.1. PRCC Tables.

Number of Exposed Cases with 100 Runs

PRCC Values	ECases	β	r_D	$\frac{1}{\tau_E}$	$\frac{1}{\tau_I}$	p	c
0.8187650246	β	0	-6.785742	-3.480713	3.746287	-0.120890	5.128212
0.9736998142	r_D	6.785742	0	3.305029	10.53203	6.664851	11.91395
0.9314292228	$\frac{1}{\tau_E}$	3.480713	-3.305029	0	7.227001	3.359823	8.608925
0.5353914372	$\frac{1}{\tau_I}$	-3.746287	-10.53203	-7.227001	0	-3.867178	1.381925
0.8245864934	p	0.120890	-6.664851	-3.359823	3.867178	0	5.249103
0.373773754	c	-5.128212	-11.91395	-8.608925	-1.381925	-5.249103	0

Table 5: PRCC values and z-values from Sensitivity Analysis for the number of Exposed cases after 100 runs.

Number of Exposed Cases with 500 Runs

PRCC Values	ECases	β	r_D	$\frac{1}{\tau_E}$	$\frac{1}{\tau_I}$	p	c
0.8350660832	β	0	-17.80147	-9.483408	6.876220	-3.052344	9.009770
0.9816410302	r_D	17.80147	0	8.318066	24.67769	14.74913	26.81124
0.947821772	$\frac{1}{\tau_E}$	9.483408	-8.318066	0	16.35963	6.4310637	18.49318
0.6444732506	$\frac{1}{\tau_I}$	-6.876220	-24.67769	-16.35963	0	-9.928564	2.133550
0.8852335403	p	3.052344	-14.74913	-6.431064	9.928564	0	12.062114
0.5577896879	c	-9.009770	-26.81124	-18.49318	-2.133550	-12.06211	0

Table 6: PRCC values and z-values from Sensitivity Analysis for the number of Exposed cases after 500 runs.

Number of Exposed Cases with 1000 Runs

PRCC Values	ECases	β	r_D	$\frac{1}{\tau_E}$	$\frac{1}{\tau_I}$	p	c
0.8151506752	β	0	-24.54984	-12.57757	10.90514	-3.069671	13.27076
0.97781069	r_D	24.54984	0	11.97227	35.45497	21.48017	37.82059
0.9363062818	$\frac{1}{\tau_I}$	12.57757	-11.97227	0	23.48271	9.507898	25.84833
0.5732090415	$\frac{1}{\tau_E}$	-10.905138	-35.45497	-23.48271	0	-13.97481	2.365620
0.8565097409	p	3.069671	-21.48017	-9.507898	13.97481	0	16.34043
0.497528456	c	-13.27076	-37.82060	-25.84833	-2.365620	-16.34043	0

Table 7: PRCC values and z-values from Sensitivity Analysis for the number of Exposed cases after 1000 runs.

Number of Exposed Cases with 2000 Runs

PRCC Values	ECases	β	r_D	$\frac{1}{\tau_E}$	$\frac{1}{\tau_I}$	p	c
0.8068706569	β	0	-25.79477	-14.02252	10.34646	-4.476775	12.64307
0.9791609255	r_D	25.79477	0	11.77224	36.14122	21.31799	38.43784
0.9411410029	$\frac{1}{\tau_E}$	14.02252	-11.77224	0	24.36898	9.545748	26.66560
0.5738147717	$\frac{1}{\tau_I}$	-10.34646	-36.14122	-24.36898	0	-14.82323	2.296618
0.8665625053	p	4.476775	-21.31799	-9.545748	14.82323	0	17.11985
0.5005341624	c	-12.64307	-38.43784	-26.66560	-2.296618	-17.11985	0

Table 8: PRCC values and z-values from Sensitivity Analysis for the number of Exposed cases after 2000 runs.

8.2. Parameter Estimation. In cases when parameters are difficult to estimate experimentally, or when we are concerned about parameter accuracy, one might be interested in estimating the value of the parameter mathematically. There are several methods for parameter estimation, including Maximum Likelihood Estimation, Bayesian Estimation, and Least Squares.

Bayesian Estimation may be the most ideal type of parameter estimation for this problem because it assumes that parameters have specific distributions, rather than having a deterministic value. In reality, our parameters will be depending on host and situation. The problem with Bayesian Estimation by itself, it is requires an educated guess as to a prior distribution, which may require some knowledge of hyperparameters for the prior distribution. We will use Maximum Likelihood Estimation in order

Number of Infectious Cases with 100 Runs

PRCC Values	ICases	β	r_D	$\frac{1}{\tau_E}$	$\frac{1}{\tau_I}$	p	c
0.8472567402	β	0	-6.964773	4.965806	-2.916505	-0.378176	4.152177
0.9792463986	r_D	6.964773	0	11.93058	4.048267	6.586596	11.11695
0.4700769672	$\frac{1}{\tau_E}$	-4.965806	-11.93058	0	-7.882312	-5.343983	-0.813629
0.9326953513	$\frac{1}{\tau_I}$	2.916505	-4.048267	7.882312	0	2.538329	7.068682
0.8623432695	p	0.378176	-6.586596	5.343983	-2.538329	0	4.530353
0.5585956599	c	-4.152177	-11.11695	0.813629	-7.068682	-4.530353	0

Table 9: PRCC values and z-values from Sensitivity Analysis for the number of infectious cases after 100 runs.

Number of Infectious Cases with 500 Runs

PRCC Values	ICases	β	r_D	$\frac{1}{\tau_E}$	$\frac{1}{\tau_I}$	p	c
0.8365559793	β	0	-17.75696	12.29364	-8.860972	-1.900536	9.352198
0.9817173522	r_D	17.75696	0	30.05060	8.895991	15.85643	27.10916
0.4011149139	$\frac{1}{\tau_E}$	-12.29364	-30.05060	0	-21.15461	-14.19417	-2.941439
0.9441677021	$\frac{1}{\tau_I}$	8.860972	-8.895991	21.15461	0	6.960436	18.21317
0.8694655814	p	1.900536	-15.85643	14.19417	-6.960436	0	11.25273
0.5460298962	c	-9.352198	-27.10916	2.941439	-18.21317	-11.25273	0

Table 10: PRCC values and z-values from Sensitivity Analysis for the number of infectious cases after 500 runs.

to find estimators for hyperparameters, such as the mean of the distribution of the parameter we wish to estimate. Maximum Likelihood Estimation was chosen over Least Squares Estimation, because Least Squares assumes that errors are normally distributed around 0; and since there may be some systematic error in the method of data collection, this may not be a reasonable assumption a priori.

8.2.1. *Maximum Likelihood Estimation.* Maximum Likelihood Estimation is useful for estimating parameters of a distribution that are most likely to provide the observed data. This type of estimation requires forming a Likelihood Function, which is the joint distribution function of each observation [30]. Given n observations, the

Number of Infectious Cases with 1000 Runs

PRCC Values	ICases	β	r_D	$\frac{1}{\tau_E}$	$\frac{1}{\tau_I}$	p	c
0.8315170275	β	0	-25.046955	16.31431	-12.40345	-2.388506	14.042700
0.9808026026	r_D	25.04695	0	41.36126	12.64350	22.65845	39.08965
0.4301893193	$\frac{1}{\tau_E}$	-16.31431	-41.36126	0	-28.71776	-18.70282	-2.271609
0.9414034042	$\frac{1}{\tau_I}$	12.40345	-12.64350	28.71776	0	10.01494	26.44615
0.861809058	p	2.388506	-22.65845	18.70282	-10.014945	0	16.43121
0.5095921386	c	-14.04270	-39.08965	2.271609	-26.44615	-16.43121	0

Table 11: PRCC values and z-values from Sensitivity Analysis for the number of infectious cases after 1000 runs.

Number of Infectious Cases with 2000 Runs

PRCC Values	ICases	β	r_D	$\frac{1}{\tau_E}$	$\frac{1}{\tau_I}$	p	c
0.8128467366	β	0	-24.86361	15.42654	-12.41065	-2.127387	13.07770
0.9781273761	r_D	24.86361	0	40.29015	12.452960	22.73622	37.94131
0.4155834083	$\frac{1}{\tau_E}$	-15.42654	-40.29015	0	-27.83719	-17.55393	-2.348834
0.934515402	$\frac{1}{\tau_I}$	12.41065	-12.45296	27.83719	0	10.28326	25.48835
0.8428499052	p	2.127387	-22.73622	17.55393	-10.28326	0	15.20509
0.4989149404	c	-13.07770	-37.94131	2.348834	-25.48835	-15.20509	0

Table 12: PRCC values and z-values from Sensitivity Analysis for the number of infectious cases after 2000 runs.

Number of Deaths due to Infection with 100 Runs

PRCC Values	IDeath	β	r_D	$\frac{1}{\tau_E}$	$\frac{1}{\tau_I}$	p	c
0.9407753838	β	0	-7.561800	7.656622	9.969193	3.228404	4.614269
0.993537033	r_D	7.561800	0	15.21842	17.53099	10.79020	12.17607
0.5438874125	$\frac{1}{\tau_E}$	-7.656622	-15.21842	0	2.312571	-4.428218	-3.042353
0.2606645725	$\frac{1}{\tau_I}$	-9.969193	-17.53099	-2.312571	0	-6.740789	-5.354924
0.8527486582	p	-3.228404	-10.79020	4.428218	6.740789	0	1.385865
0.785927044	c	-4.614269	-12.17607	3.042353	5.354924	-1.385865	0

Table 13: PRCC values and z-values from Sensitivity Analysis for the number of deaths due to infection after 100 runs.

Number of Deaths due to Infection with 500 Runs

PRCC Values	IDeath	β	r_D	$\frac{1}{\tau_E}$	$\frac{1}{\tau_I}$	p	c
0.9197543749	β	0	-18.60324	15.13875	18.63044	5.698412	10.69252
0.9922511265	r_D	18.60324	0	33.74199	37.23368	24.30165	29.29576
0.5519881377	$\frac{1}{\tau_E}$	-15.13875	-33.74199	0	3.491687	-9.440340	-4.446228
0.3785686213	$\frac{1}{\tau_I}$	-18.63044	-37.23368	-3.491687	0	-12.93203	-7.937915
0.8407547826	p	-5.698412	-24.30165	9.440340	12.93203	0	4.994111
0.7187265837	c	-10.69252	-29.29576	4.446228	7.937915	-4.994111	0

Table 14: PRCC values and z-values from Sensitivity Analysis for the number of deaths due to infection after 500 runs.

Number of Deaths due to Infection with 1000 Runs

PRCC Values	IDeath	β	r_D	$\frac{1}{\tau_E}$	$\frac{1}{\tau_I}$	p	c
0.9217810715	β	0	-26.06837	21.11024	27.77618	8.389259	16.04781
0.9922063259	r_D	26.06837	0	47.17861	53.84455	34.45763	42.11618
0.5732780552	$\frac{1}{\tau_E}$	-21.11024	-47.17861	0	6.665937	-12.72098	-5.062429
0.3389729128	$\frac{1}{\tau_I}$	-27.77618	-53.84455	-6.665937	0	-19.38692	-11.72837
0.8407918016	p	-8.389259	-34.45763	12.72098	19.38692	0	7.658554
0.7063273652	c	-16.047813	-42.116183	5.062429	11.72837	-7.658554	0

Table 15: PRCC values and z-values from Sensitivity Analysis for the number of deaths due to infection after 1000 runs.

Number of Deaths due to Infection with 2000 Runs

PRCC Values	IDeath	β	r_D	$\frac{1}{\tau_E}$	$\frac{1}{\tau_I}$	p	c
0.9163586754	β	0	-26.12393	20.29580	26.30186	8.599075	15.34169
0.9916862511	r_D	26.12393	0	46.41973	52.42580	34.72301	41.46563
0.5743929833	$\frac{1}{\tau_E}$	-20.29580	-46.41973	0	6.006065	-11.69672	-4.954103
0.3663822842	$\frac{1}{\tau_I}$	-26.30186	-52.42580	-6.006065	0	-17.70279	-10.96017
0.8272994399	p	-8.599075	-34.72301	11.69672	17.70279	0	6.742620
0.7047181159	c	-15.34169	-41.46563	4.954103	10.96017	-6.742620	0

Table 16: PRCC values and z-values from Sensitivity Analysis for the number of deaths due to infection after 2000 runs.

Number of Virons Cleared with 100 Runs

PRCC Values	Vclear	β	r_D	$\frac{1}{\tau_E}$	$\frac{1}{\tau_I}$	p	c
0.522608818	β	0	-5.354223	3.686859	-1.179973	-7.023793	-12.02889
0.8795292887	r_D	5.354223	0	9.041083	4.174251	-1.669569	-6.674662
0.03333335911	$\frac{1}{\tau_E}$	-3.686859	-9.041083	0	-4.866832	-10.71065	-15.71574
0.6380352065	$\frac{1}{\tau_I}$	1.179973	-4.174251	4.866832	0	-5.843820	-10.84891
0.9247978822	p	7.023793	1.669569	10.71065	5.843820	0	-5.005093
0.9824390488	c	12.02889	6.674662	15.71574	10.84891	5.005093	0

Table 17: PRCC values and z-values from Sensitivity Analysis for the number of virons cleared after 100 runs.

Number of Virons Cleared with 500 Runs

PRCC Values	Vclear	β	r_D	$\frac{1}{\tau_E}$	$\frac{1}{\tau_I}$	p	c
0.4579386643	β	0	-12.28207	4.578262	-5.329070	-17.25895	-28.10644
0.8561042677	r_D	12.28207	0	16.86033	6.953001	-4.976876	-15.82437
0.1997799901	$\frac{1}{\tau_E}$	-4.578262	-16.86033	0	-9.907332	-21.83721	-32.68470
0.6830528232	$\frac{1}{\tau_I}$	5.329069	-6.953001	9.907332	0	-11.92988	-22.77737
0.921096069	p	17.25895	4.976876	21.83721	11.92988	0	-10.84749
0.9796390198	c	28.10644	15.82437	32.68470	22.77737	10.84749	0

Table 18: PRCC values and z-values from Sensitivity Analysis for the number of virons cleared after 500 runs.

Number of Virons Cleared with 1000 Runs

PRCC Values	Vclear	β	r_D	$\frac{1}{\tau_E}$	$\frac{1}{\tau_I}$	p	c
0.471311629	β	0	-17.67633	7.747615	-8.051663	-24.70053	-39.64880
0.8632206436	r_D	17.67633	0	25.42395	9.624670	-7.024193	-21.97247
0.1622547445	$\frac{1}{\tau_E}$	-7.747615	-25.42395	0	-15.79928	-32.44814	-47.39642
0.7031317985	$\frac{1}{\tau_I}$	8.051663	-9.624671	15.79928	0	-16.64886	-31.59714
0.9248272022	p	24.70053	7.024193	32.44814	16.64886	0	-14.94827
0.9798160961	c	39.64880	21.97247	47.39642	31.59714	14.94827	0

Table 19: PRCC values and z-values from Sensitivity Analysis for the number of virons cleared after 1000 runs.

Number of Virons Cleared with 2000 Runs

PRCC Values	Vclear	β	r_D	$\frac{1}{\tau_E}$	$\frac{1}{\tau_I}$	p	c
0.4925516387	β	0	-18.71137	7.684263	-8.508295	-25.19609	-40.97937
0.880954189	r_D	18.71137	0	26.39564	10.20308	-6.484718	-22.26800
0.19181046	$\frac{1}{\tau_E}$	-7.684263	-26.39564	0	-16.19256	-32.88036	-48.66363
0.7266771262	$\frac{1}{\tau_I}$	8.508295	-10.20308	16.19256	0	-16.68780	-32.47108
0.9317276171	p	25.19609	6.484718	32.88036	16.68780	0	-15.78328
0.9830270668	c	40.97937	22.26800	48.66363	32.47108	15.78328	0

Table 20: PRCC values and z-values from Sensitivity Analysis for the number of virons cleared after 2000 runs.

likelihood function would take to following form:

$$L(\theta) = f(x_1|\theta) \cdot f(x_2|\theta) \cdot \dots \cdot f(x_n|\theta) = \prod_{i=1}^n f(x_i|\theta)$$

where observations are assumed to be independent and identically distributed [30, 38]. We wish to find the value of the parameter θ which provides the highest likelihood of getting the data that was observed. This can be accomplished through some simple calculus; however, the likelihood function is not always the most ideal because it is difficult to take the derivative of a repeated product. Instead, we find the log-likelihood function,

$$l(\theta) = \log(L(\theta)) = \sum_{i=1}^n \log(f(x_i|\theta))$$

and find the maximum of this new function. As logarithms are monotonic functions, $\operatorname{argmax}(l(\theta)) = \operatorname{argmax}(L(\theta))$. So, to find the maximum we set $l'(\theta) = 0$. In some

cases, θ may be a vector of the form $\begin{bmatrix} \theta_1 \\ \theta_2 \\ \vdots \\ \theta_p \end{bmatrix}$ where $\theta_1, \theta_2, \dots, \theta_p$ are each parameters of

the probability distribution f . In this case, we would need to take p partial derivatives and set each equal to 0. Like so: $\frac{\partial l}{\partial \theta_1} = 0, \frac{\partial l}{\partial \theta_2} = 0, \dots, \frac{\partial l}{\partial \theta_p} = 0$. Upon solving for

θ_i and confirming that the result is the $\text{argmax}(l(\theta_i))$; the resulting expression is the estimator of the parameter θ_i [30, 38].

8.2.2. *Bayesian Estimation.* As opposed to Maximum Likelihood Estimation, in Bayesian Estimation, each parameter that we hope to estimate is considered a random variable [30, 19]. We begin with a prior distribution, $g(\theta)$, which is an educated guess as to the distribution of the parameter, θ . There is also the option for noninformative prior in the case where we don't have any conditions for the prior distribution that our parameter should be. The prior distribution for θ will involve hyper-parameters, such as what we expect the mean of our parameter to be. For our purposes, these hyper-parameters will be informed by our maximum likelihood estimation. We will then use data to inform and adjust our prior distribution and form what is known as a posterior distribution. The posterior distribution may be thought of as the distribution of the parameter θ , given our knowledge of the data x_1, x_2, \dots, x_n ; and is written as $g(\theta|x_1, x_2, \dots, x_n)$. By implementing Bayes' Theorem, we can re-write the posterior distribution in terms of the prior [18, 30, 19].

$$g(\theta|x_1, x_2, \dots, x_n) = \frac{f(x_1, x_2, \dots, x_n|\theta)g(\theta)}{f(x_1, x_2, \dots, x_n)} = \frac{(\prod_{i=1}^n f(x_i|\theta)) g(\theta)}{\int_{\Omega} (\prod_{i=1}^n f(x_i|\theta)) g(\theta)d\theta}$$

where Λ is the parameter space. Since the denominator does not depend on θ , we may write

$$g(\theta|x_1, x_2, \dots, x_n) \propto f(x_1, x_2, \dots, x_n|\theta)g(\theta).$$

Once the posterior distribution is determined, θ may be estimated by finding its expected value

$$\hat{\theta} = \mathbb{E}(\theta) = \int_{\Lambda} \theta g(\theta|x_1, x_2, \dots, x_n)d\theta.$$

REFERENCES

- [1] Nih fact sheets - influenza.
- [2] L. Allen. *An Introduction to Stochastic Processes with Applications to Biology, Second Edition*. Chapman and Hall/CRC, 2010.
- [3] Linda J. Allen and Amy M. Burgin. Comparison of deterministic and stochastic sis and sir models in discrete time. *Mathematical Biosciences*, 163:1–33, 2000.
- [4] Linda J.S. Allen. A primer on stochastic epidemic models: Formulation, numerical simulation, and analysis. *Infectious Disease Modelling*, 2(2):128–142, 2017.
- [5] Prasith Baccam, Catherine Beauchemin, Catherine A. Macken, Frederick G. Hayden, and Alan S. Perelson. Kinetics of influenza a virus infection in humans. *Journal of Virology*, 80(15):7590–7599, 2006.
- [6] Fan Bai, Krystin E. S. Huff, and Linda J. S. Allen. The effect of delay in viral production in within-host models during early infection. *Journal of Biological Dynamics*, pages 1–27, 2018.
- [7] Catherine AA Beauchemin and Andreas Handel. A review of mathematical models of influenza a infections within a host or cell culture: lessons learned and challenges ahead. *BMC Public Health*, 11(1):S7, 2011.
- [8] G. A. Bocharov and A. A. Romanyukha. Mathematical model of antiviral immune response III. influenza a virus infection. *Journal of Theoretical Biology*, 167(4):323–360, 1994.
- [9] Fred Brauer and Carlos Castillo-Chávez. *Mathematical models in population biology and epidemiology*. Number 40 in Texts in applied mathematics. Springer, 2nd ed edition, 2012.
- [10] Yongli Cai, Yun Kang, and Weiming Wang. A stochastic SIRS epidemic model with nonlinear incidence rate. *Applied Mathematics and Computation*, 305:221–240, 2017.
- [11] AD Cliff, P Haggett, and JK Ord. *Spatial Aspects of Influenza Epidemics*. Pion Limited, 1986.
- [12] C. Coraux, R. Hajj, P. Lesimple, and E. Puchelle. In vivo models of human airway epithelium repair and regeneration. *European Respiratory Review*, 14(97):131–136, 2005.
- [13] Lynn M. Crosby and Christopher M. Waters. Epithelial repair mechanisms in the lung. *American Journal of Physiology-Lung Cellular and Molecular Physiology*, 298(6):L715–L731, 2010.
- [14] R.G. Crystal and J.B. West. *The Lung: Scientific Foundations*, volume 1. Raven Press Ltd., 2nd ed edition, 1991.
- [15] Lucas Deecke and Hana M. Dobrovolny. Intermittent treatment of severe influenza. *Journal of Theoretical Biology*, 442:129–138, 2018.
- [16] Rebekah E. Dumm, Jessica K. Fiege, Barbara M. Waring, Chay T. Kuo, Ryan A. Langlois, and Nicholas S. Heaton. Non-lytic clearance of influenza b virus from infected cells preserves epithelial barrier function. *Nature Communications*, 10(1):779, 2019.
- [17] Christina J. Edholm, Blessing O. Emerenini, Anarina L. Murillo, Omar Saucedo, Nika Shakiba, Xueying Wang, Linda J. S. Allen, and Angela Peace. Searching for superspreaders: Identifying epidemic patterns associated with superspreading events in stochastic models. In Ami Radunskaya, Rebecca Segal, and Blerta Shtylla, editors, *Understanding Complex Biological Systems*

- with Mathematics*, Association for Women in Mathematics Series, pages 1–29. Springer International Publishing, 2018.
- [18] Brian Everitt and David C. Howell, editors. *Encyclopedia of statistics in behavioral science*. John Wiley & Sons, 2005.
 - [19] Andrew Gelman, John B. Carlin, Hal S. Stern, David B. Dunson, Aki Vehtari, Donald B. Rubin, John B. Carlin, Hal S. Stern, David B. Dunson, Aki Vehtari, and Donald B. Rubin. *Bayesian Data Analysis*. Chapman and Hall/CRC, 2013.
 - [20] Connie Goldsmith. *Influenza: The Next Pandemic?* Twenty-First Century Books, 2007.
 - [21] Bolye Gomero. Latin hypercube sampling and partial rank correlation coefficient analysis applied to an optimal control problem. 2012.
 - [22] Jennifer R. Hamilton, David Sachs, Jean K. Lim, Ryan A. Langlois, Peter Palese, and Nicholas S. Heaton. Club cells surviving influenza a virus infection induce temporary nonspecific antiviral immunity. *Proceedings of the National Academy of Sciences*, 113(14):3861–3866, 2016.
 - [23] Adriana Heguy, Ben-Gary Harvey, Philip L. Leopold, Igor Dolgalev, Tina Raman, and Ronald G. Crystal. Responses of the human airway epithelium transcriptome to in vivo injury. *Physiological Genomics*, 29(2):139–148, 2007.
 - [24] Benjamin P. Holder and Catherine AA Beauchemin. Exploring the effect of biological delays in kinetic models of influenza within a host or cell culture. *BMC Public Health*, 11(1):S10, 2011.
 - [25] Arie Hordijk, Donald L Iglehart, and Rolf Schassberger. Discrete time methods for simulating continuous time markov chains. *Cambridge University Press*, page 18, 1976.
 - [26] Ivan Ivanov and Edward R. Dougherty. Modeling genetic regulatory networks: continuous or discrete? *Journal of Biological Systems*, 14(2):219–229, 2006.
 - [27] P. D. Jones and G. L. Ada. Influenza virus-specific antibody-secreting cells in the murine lung during primary influenza virus infection. *Journal of Virology*, 60(2):614–619, 1986.
 - [28] Matthew James Keeling and Pejman Rohani. *Modeling infectious diseases in humans and animals*. Princeton University Press, 2008. OCLC: ocn163616681.
 - [29] Bonnie E. Lai, Marcus H. Henderson, Jennifer J. Peters, David K. Walmer, and David F. Katz. Transport theory for HIV diffusion through in vivo distributions of topical microbicide gels. *Biophysical Journal*, 97(9):2379–2387, 2009.
 - [30] Richard J. Larsen and Morris L. Marx. An introduction to mathematical statistics and its applications: Fifth edition. *The American Statistician*, page 00031305.2011.645758, 2011.
 - [31] Michael Li. *An Introduction to Mathematical Modeling of Infectious Diseases*. Number 2 in Mathematics of Planet Earth. Springer, 2018.
 - [32] Tufail Malik. Discrete time markov chain of a dynamical system with a rest phase. *International Journal of Applied Nonlinear Science*, 2:137, 01 2016.

- [33] Simeone Marino, Ian B Hogue, Christian J Ray, and Denise E Kirschner. A methodology for performing global uncertainty and sensitivity analysis in systems biology. *Journal of theoretical biology*, 254(1):178–196, 2008.
- [34] Mikhail Matrosovich, Tatyana Matrosovich, Jennifer Uhlenorff, Wolfgang Garten, and Hans-Dieter Klenk. Avian-virus-like receptor specificity of the hemagglutinin impedes influenza virus replication in cultures of human airway epithelium. *Virology*, 361(2):384–390, 2007.
- [35] Mikhail N. Matrosovich, Tatyana Y. Matrosovich, Thomas Gray, Noel A. Roberts, and Hans-Dieter Klenk. Human and avian influenza viruses target different cell types in cultures of human airway epithelium. *Proceedings of the National Academy of Sciences*, 101(13):4620–4624, 2004.
- [36] Hongyu Miao, Joseph A. Hollenbaugh, Martin S. Zand, Jeanne Holden-Wiltse, Tim R. Mosmann, Alan S. Perelson, Hulin Wu, and David J. Topham. Quantifying the early immune response and adaptive immune response kinetics in mice infected with influenza a virus. *Journal of Virology*, 84(13):6687–6698, 2010.
- [37] Rui-Xing Ming, Jiming Liu, William K. W. Cheung, and Xiang Wan. Stochastic modelling of infectious diseases for heterogeneous populations. *Infectious Diseases of Poverty*, 5(1):107, 2016.
- [38] In Jae Myung. Tutorial on maximum likelihood estimation. *Journal of Mathematical Psychology*, 47(1):90–100, 2003.
- [39] J. M. Nicholls, M. C. W. Chan, W. Y. Chan, H. K. Wong, C. Y. Cheung, D. L. W. Kwong, M. P. Wong, W. H. Chui, L. L. M. Poon, S. W. Tsao, Y. Guan, and J. S. M. Peiris. Tropism of avian influenza a (h5n1) in the upper and lower respiratory tract. *Nature Medicine*, 13(2):147, 2007.
- [40] Hiroshi Nishiura. Real-time forecasting of an epidemic using a discrete time stochastic model: a case study of pandemic influenza (h1n1-2009). *BioMedical Engineering OnLine*, 10(1):15, 2011.
- [41] Navavat Pipatsart, Wannapong Triampo, and Charin Modchang. Stochastic models of emerging infectious disease transmission on adaptive random networks. *Computational and Mathematical Methods in Medicine*, 2017:1–11, 2017.
- [42] C.W. Potter. *Principles and Practice of Clinical Virology*. John Wiley & Sons, 5th ed edition, 2004.
- [43] Roberto A. Saenz, Michelle Quinlivan, Debra Elton, Shona MacRae, Anthony S. Blunden, Jennifer A. Mumford, Janet M. Daly, Paul Digard, Ann Cullinane, Bryan T. Grenfell, John W. McCauley, James L. N. Wood, and Julia R. Gog. Dynamics of influenza virus infection and pathology. *Journal of Virology*, 84(8):3974–3983, 2010.
- [44] Andrea Saltelli, Marco Ratto, Terry Andres, Francesca Campolongo, Jessica Cariboni, Debora Gatelli, Michaela Saisana, and Stefano Tarantola. *Global Sensitivity Analysis. The Primer*. John Wiley & Sons, Ltd, 2007.

- [45] Werner Sandmann. Discrete-time stochastic modeling and simulation of biochemical networks. *Computational Biology and Chemistry*, 32(4):292–297, 2008.
- [46] Amber M. Smith. Host-pathogen kinetics during influenza infection and coinfection: insights from predictive modeling. *Immunological Reviews*, 285(1):97–112, 2018.
- [47] Pauline van de Driessche and James Watmough. Reproduction numbers and sub-threshold endemic equilibria for compartmental models of disease transmission. *Mathematical Biosciences*, 180:29–48, 2002.
- [48] Debby van Riel, Vincent J. Munster, Emmie de Wit, Guus F. Rimmelzwaan, Ron A. M. Fouchier, Albert D. M. E. Osterhaus, and Thijs Kuiken. Human and avian influenza viruses target different cells in the lower respiratory tract of humans and other mammals. *The American Journal of Pathology*, 171(4):1215–1223, 2007.
- [49] David Warburton, Laura Perin, Roger DeFilippo, Saverio Bellusci, Wei Shi, and Barbara Driscoll. Stem/progenitor cells in lung development, injury repair, and regeneration. *Proceedings of the American Thoracic Society*, 5(6):703–706, 2008.
- [50] Stephen Wiggins. *Introduction to Applied Nonlinear Dynamical Systems and Chaos*, volume 2 of *Texts in Applied Mathematics*. Springer, second edition, 2003.
- [51] D. L. Wilhelm. Regeneration of tracheal epithelium. *The Journal of Pathology and Bacteriology*, 65(2):543–550, 1953.
- [52] Ada W. C. Yan, Pengxing Cao, and James M. McCaw. On the extinction probability in models of within-host infection: the role of latency and immunity. *Journal of Mathematical Biology*, 73(4):787–813, 2016.
- [53] Lu Yao, Christine Korteweg, Wei Hsueh, and Jiang Gu. Avian influenza receptor expression in h5n1-infected and noninfected human tissues. *The FASEB Journal*, 22(3):733–740, 2007.
- [54] Nada P Younis. A SPATIAL MODEL FOR THE SPREAD OF INFLUENZA WITHIN THE HUMAN RESPIRATORY TRACT. *Ryerson University Press*, page 62, 2012.
- [55] Lei Zhao, Ali B Abbasi, and Christopher J R Illingworth. Mutational load causes stochastic evolutionary outcomes in acute RNA viral infection. *Virus Evolution*, 5(1), 2019.
- [56] Shufa Zheng, Lingling Tang, Hainv Gao, Yiyin Wang, Fei Yu, Dawei Cui, Guoliang Xie, Xianzhi Yang, Wen Zhang, Xianfei Ye, Zike Zhang, Xi Wang, Liang Yu, Yiming Zhang, Shigui Yang, Weifeng Liang, Yu Chen, and Lanjuan Li. Benefit of early initiation of neuraminidase inhibitor treatment to hospitalized patients with avian influenza a(h7n9) virus. *Clinical Infectious Diseases*, 66(7):1054–1060, 2017.

NEW PALTZ STATE UNIVERSITY OF NEW YORK

E-mail address: williamc18@hawkmail.newpaltz.edu

UNIVERSITY OF OREGON

E-mail address: kristaw@uoregon.edu